Effect of Screened Nuclei on Fast Electron Beam Dynamics

Master's thesis in Physics and Astronomy

LINNEA HESSLOW

Effect of Screened Nuclei on Fast Electron Beam Dynamics

LINNEA HESSLOW

Effect of Screened Nuclei on Fast Electron Beam Dynamics
LINNEA HESSLOW

Supervisor: Ola Embréus, Department of Physics
Examiner: Tünde Fülöp, Department of Physics

Cover: A plasma globe, which is a glass sphere filled with noble gases equipped with
a high-voltage electrode at its center.
© User:Colin / Wikimedia Commons /CC-BY-SA-3.0/ https://commons.wikimedia.
org/wiki/File%3APlasma_globe_60th.jpg.

Typeset in LaTeX
Gothenburg, Sweden 2016

Effect of Screened Nuclei on Fast Electron Beam Dynamics
LINNEA HESSLOW
Department of Physics
Chalmers University of Technology

Abstract

In a plasma, particles can be accelerated to relativistic speeds by an electric field. These relativistic particles are of importance to, for example, fusion research, where they pose a risk of damaging the walls of a reactor. In order to understand the dynamics of runaway particles, the Coulomb interaction between particles ("collisions") is a central concept. In this thesis we focus on the collisions between particles and partially ionized ions. The interaction strength depends on the incoming particle momentum: at low momentum the nucleus is screened by the bound electrons and the net ion charge will define the interaction strength; at high momentum the particle may penetrate the electron cloud around the nucleus and the relevant charge is then the nuclear charge. Since the collision cross section is proportional to the charge squared, this can be expected to have a significant impact on the runaway dynamics.

In this thesis we investigate the energy dependence of screening. Starting from a quantum mechanical collision cross section, we derive the form of the Fokker–Planck collision operator appropriate for the many-body plasma system. When accurately accounting for screening, we find that the collision rates can be significantly enhanced compared to the fully screened case, in particular at high momentum. Furthermore, we derive general forms of the high energy behavior of the collision frequencies, which hold regardless of the details of the model used to describe the electron cloud of the ion. Finally, we find indications that the use of the Fokker–Planck operator might have to be improved by considering the Boltzmann operator, in order to take large-angle collisions into account.

Acknowledgements

Contents

Contents

x

1

Introduction

A vast majority of the known matter in the universe is in the plasma state [1]. Commonly referred to as the fourth state of matter, a plasma is an ionized gas with sufficiently high density of charged particles that the electric field of an individual particle is screened by the others on macroscopic scales – that is, the plasma is quasineutral. Even though not commonly encountered on Earth due to the low temperature in relation to the particle density, plasma physics is an important component in a wide range of areas including astrophysics, fusion reactors and laser physics.

An intriguing effect in plasma physics is the creation of runaway particles, most often runaway electrons. Collisions in a plasma are rather different from the experience of everyday life; the friction force on a fast plasma particle *decreases* with increased speed [2]. That is as if the drag force would decrease the faster a cyclist bikes, leading to an indefinite acceleration if a constant force is applied, until relativistic speeds are reached. Runaway electrons can thus arise in the presence of an accelerating electric field when this field exceeds a critical electric field. Situations where these fields are present and where runaway electrons are believed to be important include solar flares and thunderstorms, as well as tokamak disruptions [3, 4]. A tokamak is a torus-shaped device employed in fusion research which uses a strong magnetic field and toroidal plasma current to confine the plasma. A central problem to the operation of tokamaks is the risk of plasma-terminating disruptions. During a disruption, instabilities in the magnetized fluid lead to a rapid cooling of the plasma and a plasma current termination, which can induce a strong electric field. This poses a significant problem in fusion research as highly energetic runaways can be generated and may damage the walls of the reactors [5].

The description of plasma particle collisions is an essential element of understanding runaway dynamics. The Coulomb interaction between plasma particles can be modeled as a combination of the effects of short-scale collisions and the long-scale effects of the average, or screened, electromagnetic field in the quasineutral plasma (note the distinction between the short-scale screening of a nucleus by the cloud of bound electrons – the topic of this thesis – and the long-scale screening of a localized charge fluctuation by the surrounding plasma). In all of the above mentioned areas, scenarios are of interest where the plasma contains partially ionized heavy ions. In this case it is not *a priori* clear what charge should be used to model the Coulomb interaction strength of collisions with this species. One option is to assume that the colliding particles never come close to each other in relation to the scale of the

ion. The ion can then be treated as a point particle of charge $Z_0 = Z - N_e$, where the charge of the nucleus with atomic number Z is said to be screened by the N_e bound electrons. On the other hand, an energetic particle passing near the ion may penetrate the electron cloud around the nucleus. This will reduce the screening effect, and consequently the interaction strength will be higher and approach the limit where Z represents the interaction strength. Facing the range from full screening, corresponding to Z_0, to no screening, corresponding to Z, the typical choice, for example in fusion plasma physics, has been to model such a system using full screening [2, 6]. While it is appropriate at low momentum, full screening may be expected to give too weak an interaction strength at high momentum. Since the collision cross section is proportional to the charge squared [2], there could be a big difference between full screening and complete penetration of the ion, in particular for high-Z ions with a low ionization degree. This can in turn affect runaway electron dynamics. The investigation of this issue is the primary concern of this thesis.

The phenomenon of runaways was discovered in 1925 by Wilson [7], however the theory was not developed until the 1960s, starting with Drecier [8, 9]. Kruskal and Bernstein presented a classic, analytic calculation of the runaway population growth rate due to an electric field, which used an asymptotic matching across five different regions of velocity space [10]. Accounting for relativistic corrections, Connor and Hastie later found that a minimum, critical electric field is needed to accelerate even high energy particles [11]. This phenomenon is known as primary generation and these analytical results were first confirmed in numerical simulations by Kulsrud et al. [12]. The results showed that the growth of runaway electrons is very sensitive to the electric field strength. For a strong electric field, the entire electron population can run away in this manner. Conversely, for relatively weak fields though exceeding the critical field, only a very small fraction of the electrons (assuming an initial thermal population with a Maxwellian distribution) will be fast enough to run away by primary generation. The small growth rate can however be significantly enhanced by the secondary, avalanche effect, where knock-on collisions between runaway and bulk electrons can kick bulk electrons into the runaway region [13].

Runaway electrons have potential to seriously damage tokamaks, especially in ITER, which will be the world's largest tokamak experiment and is currently under construction [14]. Very strong (multi-MA) runaway currents are expected to form if a disruption is not mitigated in ITER, larger than in any present experiment [5]. Therefore, failsafe methods to deal with such currents are required. One approach is to dissipate the runaway electron currents by injecting heavy gases, for example argon or neon. They weakly ionize in the cold ($\sim 5\,\mathrm{eV}$) post-disruption plasma and act to collisionally deflect particles in the high energy electron beam. Experiments have shown that particularly gases with high atomic mass can shift the energy distribution of the electrons toward lower energy, to a much larger extent than would be predicted by the current theory of runaway electrons [5, 15]. The effect seen was stronger the higher the atomic mass of the ion, even though the ions were usually singly ionized. Therefore, the current hypothesis is that an energetic electron experiences not the fully screened, net charge of the ion, but also probes the internal structure of the atom, as mentioned above. The fast electrons would therefore

experience higher collision rates, which would be consistent with the experimental observation.

Existing theoretical works in this area do not offer easily accessible derivations of their results [16–20]. In Ref. [16], a non-quantum mechanical approach is employed to describe the effect of screening. In a formalism developed in Ref [21], collisions with bound electrons and collisions with a naked nuclei are treated separately. In contrast, the authors of Refs. [17–20] find the energy dependence of the screening from the Thomas–Fermi model, which derives the electronic structure of an ion from a semi-classical approach. The Thomas–Fermi model is simple and practical to use, but has known limitations – it describes neither atomic shell structure, nor reproduces the correct asymptotic behavior of the bound electron density at small or large distances from the nucleus [22]. The results presented in [16–20] from these two different approaches to modeling the electron density of the ion do not agree qualitatively, and none of the three references have discussed the work of the others.

It is therefore valuable to produce a clear and rigorous derivation of the collision operator, using a quantum mechanical description of the scattering process to account for the screening effect of bound electrons. Furthermore, an analysis of the robustness of the results to the assumed electron density model, as well as a test of the impact of energy transfer in the collisions, which was not considered in previous work, would be of interest.

We take a fully theoretical approach to the screening problem to establish the grounds for further study. The points raised above are addressed in this thesis as follows. In Chapter 2 the necessary background in kinetic theory for plasmas and the use of collision operators is given, together with a presentation of the quantum mechanical effects on the collision cross sections of plasma particles. Elastic collisions with ions are considered, while inelastic collisions are outside the scope of this thesis. This is applied in Chapter 3 to the non-relativistic case, where we develop a model of the full electron-ion collision operator that takes screening into account. Then in Chapter 4 we generalize these results to the relativistic case necessary to describe fully the high-energy runaway particles of interest, restricted to the limit of infinite ion mass compared to the electron mass. Finally, the conclusions are summarized in Chapter 5.

2

Kinetic Theory of Collisions in a Plasma

The two main approaches to model a plasma are fluid theory and the more complicated kinetic theory, from which the fluid theory can be rigorously derived. While the plasma parameters in the fluid theory approach only depend on three spatial variables and time, the phase space of kinetic theory consists of six variables: three velocity components and three spatial components. Accordingly, the non-Maxwellian distributions typical for runaway electrons can be treated in detail in kinetic theory. This chapter presents a brief introduction to the kinetic theory of plasmas with a focus on collisions. The classical Rutherford collisional cross section, and the resulting collision operator, are re-derived and constitute the starting point of this thesis. Quantum mechanical corrections to the cross section are then considered for both the non-relativistic and the relativistic regimes of the colliding particles. These are used in Chapters 3 and 4 to account for the effect of screening in electron-ion collisions.

2.1 Collisions in kinetic theory

The Fokker–Planck collision operator is a fundamental part of plasma physics as it describes the effect of the small-angle collisions that dominate in a hot quasineutral plasma. Though it can be derived from first principles taking many-body interactions into account, the Fokker–Planck equation can also be obtained as the small-angle limit of the Boltzmann equation, which governs the dynamics of two-body interactions.

The use of the Fokker–Planck operator in a plasma has known limits of validity. The infinite range of Coulomb interactions calls for a collision operator that accounts for many-body interactions, which are described by the Fokker–Planck operator. On the other hand, the secondary generation of runaway electrons mentioned in the Introduction indicates that large-angle collisions cannot always be neglected, and these collisions cannot be described by the Fokker–Planck operator. An approach which has been used in fusion research to treat this dilemma is to use the simpler Fokker–Planck operator for the general dynamics, and then treat collisions with energetic particles using a simplified Boltzmann operator to describe the avalanche effect [13].

This section reviews both the Boltzmann and the Fokker–Planck collision operators. The Fokker–Planck operator is derived from the Boltzmann operator non-relativistically. The similar but more involved derivation including relativistic corrections can be found in literature [23] and we simply present the resulting operator.

2.1.1 The Boltzmann equation

We begin by motivating the structure of the Boltzmann operator, following the presentation of Montgomery [24]. The Boltzmann operator appears in the kinetic equation for a species as follows. We consider the number density of a given species in an infinitesimal volume of phase space. By following the evolution of this small volume element in time, we may attribute the change in number density of the volume element to collisions.

During a time δt, the particle coordinates in absence of collisions will change to

$$\mathbf{x}' = \mathbf{x} + \mathbf{v}\delta t, \tag{2.1}$$

$$\mathbf{v}' = \mathbf{v} + \frac{\mathbf{F}}{m}\delta t, \tag{2.2}$$

where $\mathbf{F}$ is an external force acting on the ensemble. Given the species' distribution function $f(\mathbf{x},\mathbf{v},t)$, with the number density $n(\mathbf{x},t) = \int d\mathbf{v} f$, we consider the number of particles dn in the small phase space volume. Without any interaction we can use the Liouville theorem, stating that a phase space distribution is conserved along the trajectories of a system,

$$dn = dn' = f(\mathbf{x}',\mathbf{v}',t+\delta t)d\mathbf{x}'d\mathbf{v}'. \tag{2.3}$$

As $d\mathbf{x}'d\mathbf{v}' = d\mathbf{x}d\mathbf{v}$, we can perform an expansion of the distribution function which gives

$$\left(\frac{dn'-dn}{\delta t}\right)\delta t\, d\mathbf{x} = \left(\frac{\partial f}{\partial t} + \mathbf{v}\cdot\nabla_{\mathbf{x}}f + \frac{\mathbf{F}}{m}\cdot\nabla_{\mathbf{v}}f\right)\delta t\, d\mathbf{x}d\mathbf{v}. \tag{2.4}$$

Attributing the difference to the collisional interactions, we find the Boltzmann equation:

$$\frac{\partial f}{\partial t} + \mathbf{v}\cdot\nabla_{\mathbf{x}}f + \frac{\mathbf{F}}{m}\cdot\nabla_{\mathbf{v}}f = \left(\frac{\partial f}{\partial t}\right)_c. \tag{2.5}$$

To obtain the Boltzmann collision operator $(\partial f/\partial t)_c$, consider a collision between two particles. Denote the initial particle velocities as $\mathbf{v}$, $\mathbf{v}'$, and let them transform into the final states $\mathbf{v}_f$, $\mathbf{v}'_f$.

First consider the number of particles with velocity $\mathbf{v}$ that are scattered out of this region when they are hit by particles of velocity $\mathbf{v}'$. In the center of mass frame, we may parametrize a scattering event by the impact parameter b, the deflection angle θ and the azimuthal angle φ, so that the solid angle is $d\Omega = \sin\theta d\theta d\varphi$. The flux of particles into the area $b\, db\, d\varphi$ is then given by

$$b\, db\, d\varphi f(\mathbf{x},\mathbf{v}',t)|\mathbf{v} - \mathbf{v}'|d\mathbf{v}', \tag{2.6}$$

while the number of target particles – that will be scattered out of the phase space region – is $f(\mathbf{x},\mathbf{v},t)d\mathbf{v}$ within the velocity interval $[\mathbf{v}, \mathbf{v}+d\mathbf{v}]$. Utilizing the definition of solid angle, we can rewrite the expressions in terms of the differential cross section $d\sigma/d\Omega$:

$$\frac{d\sigma}{d\Omega}d\Omega = b\,db\,d\varphi. \tag{2.7}$$

The number of scattered particles out of the interval $[\mathbf{v}, \mathbf{v}+\mathbf{dv}]$ is

$$d\Omega\frac{d\sigma}{d\Omega}f(\mathbf{v})f(\mathbf{v}')|\mathbf{v}-\mathbf{v}'|, \tag{2.8}$$

which gives

$$\left(\frac{\partial f}{\partial t}\right)_{c,out} = \int d\mathbf{v}'d\Omega\frac{d\sigma}{d\Omega}f(\mathbf{v})f(\mathbf{v}')|\mathbf{v}-\mathbf{v}'|. \tag{2.9}$$

Turning to the scattering into the same velocity range, eq. (2.8) gives by symmetry

$$d\mathbf{v}'\left(d\Omega\frac{d\sigma}{d\Omega}\right)_f f(\mathbf{v}_f)f(\mathbf{v}'_f)|\mathbf{v}_f-\mathbf{v}'_f|. \tag{2.10}$$

The transformation from $\mathbf{v},\mathbf{v}'$ to $\mathbf{v}_f,\mathbf{v}'_f$ is orthogonal, and therefore

$$d\mathbf{v}d\mathbf{v}' = d\mathbf{v}_f d\mathbf{v}'_f. \tag{2.11}$$

By symmetry in the collision it is also true that[1]

$$\left(\frac{d\sigma}{d\Omega}d\Omega\right) = \left(\frac{d\sigma}{d\Omega}d\Omega\right)_f. \tag{2.12}$$

Analogously with eq. (2.9):

$$\left(\frac{\partial f}{\partial t}\right)_{c,in} = \int d\mathbf{v}'d\Omega\frac{d\sigma}{d\Omega}f(\mathbf{v}_f)f(\mathbf{v}'_f)|\mathbf{v}_f-\mathbf{v}'_f|. \tag{2.13}$$

Finally then we have the Boltzmann operator by subtracting the particles scattered out from the particles scattered in:

$$\left(\frac{\partial f}{\partial t}\right)_c = \int d\mathbf{v}'d\Omega\frac{d\sigma}{d\Omega}\Big(f(\mathbf{v}_f f(\mathbf{v}'_f) - f(\mathbf{v})f(\mathbf{v}'))\Big)|\mathbf{v}-\mathbf{v}'|. \tag{2.14}$$

Many interesting results can be obtained from the Boltzmann collision operator. For example it leads to the H theorem, that is, a system which is not in equilibrium will evolve such that entropy is increased until the equilibrium distribution of a Maxwellian (see eq. (2.75)) is reached [25].

---

[1]These two relations do not hold in the relativistic case; however, the combined quantity $d\mathbf{v}d\mathbf{v}'\left(\frac{d\sigma}{d\Omega}d\Omega\right)$ is conserved in the collision.

2.1.2   The Fokker–Planck collision operator

The Fokker-Planck operator can be elegantly obtained from the small deflection angle limit of the Boltzmann operator as we will show here. A small deflection angle corresponds to small changes in momentum of the colliding particles. This is a distinguishing feature of motion under the influence of inverse-square forces. Since an inverse-square force has infinite range, many particles will contribute with small deflections to the trajectory of a particle. By contrast, the forces between the particles in an ordinary gas decrease rapidly with distance leading to sharp deflections between almost straight trajectory segments, unlike the smooth Coulomb trajectories. In the following derivation, the small-angle limit motivates Taylor expansion in the momentum change. In Sections 2.2.2 and 2.2.3 these statements will be quantified.

Note the derivation from the Boltzmann operator is somewhat specialized, as the Fokker-Planck formalism is valid also for n-body interaction in contrast to the binary collisions required for the Boltzmann operator. This can be proved by a more general derivation of the Fokker–Planck operator utilizing methods from statistical mechanics [24]. Intuitively, this property can be understood by arguing that if every single collision contributes infinitesimally to a change in momentum, these infinitesimal contributions can be added linearly to describe many-body interactions.

To derive the Fokker-Planck operator, we start by introducing an arbitrary, smooth and differentiable function $\phi(\mathbf{v})$ and form the functional $J\{\phi\}$ by integrating the Boltzmann operator in eq. (2.14) multiplied by $\phi(\mathbf{v})$ over velocity space,

$$J\{\phi\} = \int d\mathbf{v}\phi(\mathbf{v})\left(\frac{\partial f}{\partial t}\right)_c$$
$$= \int d\mathbf{v}d\mathbf{v}'d\Omega\,\phi(\mathbf{v})\frac{d\sigma}{d\Omega}\Big(f(\mathbf{v}_f)f(\mathbf{v}'_f) - f(\mathbf{v})f(\mathbf{v}')\Big)|\mathbf{v}-\mathbf{v}'|. \qquad (2.15)$$

Once again using eqs. (2.11) and (2.12), and noting that conservation of energy and momentum gives $|\mathbf{v}-\mathbf{v}'| = |\mathbf{v}_f - \mathbf{v}'_f| \equiv u$, we can rewrite eq. (2.15) as

$$J\{\phi\} = \int d\mathbf{v}_f d\mathbf{v}'_f d\Omega\,\phi(\mathbf{v})\frac{d\sigma}{d\Omega}f(\mathbf{v}_f)f(\mathbf{v}'_f)u$$
$$- \int d\mathbf{v}d\mathbf{v}'d\Omega\,\phi(\mathbf{v})\frac{d\sigma}{d\Omega}f(\mathbf{v})f(\mathbf{v}')u$$
$$= \int d\mathbf{v}d\mathbf{v}'d\Omega\Big[\phi(\mathbf{v}_f) - \phi(\mathbf{v})\Big]\frac{d\sigma}{d\Omega}f(\mathbf{v})f(\mathbf{v}')u, \qquad (2.16)$$

where in the last step in the first term we relabeled $\mathbf{v},\mathbf{v}' \leftrightarrow \mathbf{v}_f,\mathbf{v}'_f$ which is allowed by symmetry in the initial and final states. With $J\{\phi\}$ in this form, we use the property of small momentum change to perform a Taylor expansion of ϕ in the parameter $\mathbf{v}_f - \mathbf{v} = \Delta v$. To second order, we get

$$J\{\phi\} \approx \int d\mathbf{v}d\mathbf{v}'d\Omega\frac{d\sigma}{d\Omega}f(\mathbf{v})f(\mathbf{v}')u\Big[\Delta v^\mu\nabla_\mu\phi(\mathbf{v}) + \frac{1}{2}\Delta v^\mu\Delta v^\nu\nabla_\mu\nabla_\nu\phi(\mathbf{v})\Big]$$
$$= \int d\mathbf{v}\phi(\mathbf{v})\Big[-\nabla_\mu\Big(f(\mathbf{v})\int d\mathbf{v}'d\Omega f(\mathbf{v}')\frac{d\sigma}{d\Omega}u\Delta v^\mu\Big)$$
$$+ \frac{1}{2}\nabla_\mu\nabla_\nu\Big(f(\mathbf{v})\int d\mathbf{v}'d\Omega f(\mathbf{v}')\frac{d\sigma}{d\Omega}u\Delta v^\mu\Delta v^\nu\Big)\Big], \qquad (2.17)$$

where the Greek indices μ and ν denote the three spatial degrees of freedom. Since this equation holds for arbitrary $\phi(\mathbf{v})$, we must have equivalence between the integrands of eqs. (2.15) and (2.17), and we arrive at the Fokker–Planck equation for the distribution function f_a of species a:

$$\left(\frac{\partial f_a}{\partial t}\right)_c = -\nabla_\mu \left(f_a \langle \Delta v^\mu \rangle_a\right) + \frac{1}{2} \nabla_\mu \nabla_\nu \left(f_a \langle \Delta v^\mu \Delta v^\nu \rangle_a\right), \tag{2.18}$$

where the operation of $\langle \ldots \rangle$ gives an average per unit time due to collisions with all species b; note the following expression has dimensions of (velocity time^{-1})

$$\langle \Delta v^\mu \rangle_a = \sum_b \int d\mathbf{v}' f_b(\mathbf{v}') \int d\Omega \frac{d\sigma}{d\Omega} u \Delta v^\mu, \tag{2.19}$$

and

$$\langle \Delta v^\mu \Delta v^\nu \rangle_a = \sum_b \int d\mathbf{v}' f_b(\mathbf{v}') \int d\Omega \frac{d\sigma}{d\Omega} u \Delta v^\mu \Delta v^\nu. \tag{2.20}$$

A fundamental issue here is the following: what is the reason to cut the operator after the second term? The more rigorous derivation of the Fokker–Planck operator shows that for small-angle collisions, only the terms of the first two orders will contribute.

2.1.3 Relativistic Fokker–Planck operator

The relativistic version of the Fokker–Planck collision operator in eq. (2.18) can for example be derived from the relativistic Boltzmann operator analogously to Section 2.1.2, as was done by Akama [23]. Unlike the non-relativistic Fokker–Planck operator, the relativistic form has not been derived from first principles independently from the Boltzmann operator.

The relativistic collision operator reads, analogously to the non-relativistic case

$$\left(\frac{\partial f_a}{\partial t}\right)_c = -\nabla_i \left(f_a \langle \Delta p^i \rangle_a\right) + \frac{1}{2} \nabla_i \nabla_j \left(f_a \langle \Delta p^i \Delta p^j \rangle_a\right), \tag{2.21}$$

where the derivatives are taken with respect to the incoming momentum $p^i = (E/c, \mathbf{p}) = \gamma m(c, \mathbf{v})$ and $i, j, \cdots = 0,1,2,3$ for all the four components of spacetime. Analogously to the notation above, the collision kinematics between species a and b is described by the momenta $p^i, (p')^i \to p_f^i, (p_f')^i$; the distribution function $f(p^i)$ is now a function of momentum rather than velocity. Scalar products are given in the $-+++$ signature, and the usage of t instead of the proper time τ in eq. (2.21) is compensated by the Lorentz factor $\gamma = p^0$ in the brackets below.

The brackets are given by

$$\langle \Delta p^i \rangle_a = \sum_b \int d\mathbf{p}' f_b(p'^l) \int d\Omega \frac{d\sigma}{d\Omega} c \frac{\sqrt{(p^k p_k')^2 - m_a^2 m_b^2 c^4}}{(p^0)' p^0} \Delta p^i, \tag{2.22}$$

$$\langle \Delta p^i \Delta p^j \rangle_a = \sum_b \int d\mathbf{p}' f_b(p'^l) \int d\Omega \frac{d\sigma}{d\Omega} c \frac{\sqrt{(p^k p_k')^2 - m_a^2 m_b^2 c^4}}{(p^0)' p^0} \Delta p^i \Delta p^j. \tag{2.23}$$

Apart from the relative velocity u being replaced by a more complicated formula for the same quantity, there are no major differences to the non-relativistic case, and the non-relativistic quantities are replaced by their relativistic counterparts. Note that the collision operator is not manifestly relativistically invariant; only the product of the cross section and relative velocity is invariant.

2.2 Collisions due to a Coulomb interaction

From general collision operators, we now move on to the special case of the Coulomb interaction. This section presents the typical (fully screened) treatment, therefore without any quantum mechanical corrections. It also neglects relativistic effects. In re-deriving the expressions for the Fokker–Planck operator, the formalism used in later chapters is developed. The concept of the Coulomb logarithm is also explained, as well as the linearized collision operator and how it gives rise to runaway electrons.

2.2.1 Rutherford cross section

The typical cross section used for the collision operator in plasma physics is the Rutherford cross section, the cross section obtained in the non-relativistic regime for a two-particle Coulomb interaction. In the following paragraphs we derive the Rutherford cross section for the case where both particles have finite mass and therefore accounting for the recoil of the target particle, as opposed to the version where a light particle (electron) collides with a stationary heavy particle (ion). The resulting formula serves as the starting point when the electron density around the ion is later taken into account. The main ingredients for this derivation may be found in Helander and Sigmar [2]. Throughout this thesis we consider the *differential cross section $d\sigma/d\Omega$*; since this is clear from the context we consistently refer to it in the shorter form *cross section*.

We make a transformation to describe the system as a particle with the reduced mass m_{ab} interacting with a stationary particle in the center of mass frame. The Lagrangian for a particle a at position $\mathbf{x}_a$ with mass m_a and charge $e_a = -e$, and similarly particle b at $\mathbf{x}_b$ with mass m_b and charge $e_b = Z_0 e$ interacting electrostatically, is

$$\mathscr{L} = \frac{m_a \dot{\mathbf{x}}_a^2}{2} + \frac{m_b \dot{\mathbf{x}}_b^2}{2} + \frac{Z_0 m_e r_0 c^2}{|\mathbf{x}_a - \mathbf{x}_b|}. \tag{2.24}$$

Here we parametrize the constants with the classical electron radius r_0,

$$r_0 m_e c^2 = \frac{e^2}{4\pi\epsilon_0}, \tag{2.25}$$

where $r_0 = \alpha^2 a_0$, $a_0 = \hbar/(m_e c \alpha)$ is the Bohr radius and $\alpha = e^2/(4\pi\epsilon_0 \hbar c) \approx 1/137$ is the fine-structure constant. With this choice of constants, the dimensions of the quantities are manifest, which will be particularly useful in later chapters.

We now introduce the center of mass and relative position vectors

$$\mathbf{R} = \frac{m_a \mathbf{x}_a + m_b \mathbf{x}_b}{m_a + m_b}, \tag{2.26}$$

$$\mathbf{r} = \mathbf{x_a} - \mathbf{x}_b, \tag{2.27}$$

giving

$$\frac{m_a \dot{\mathbf{x}}_a^2}{2} + \frac{m_b \dot{\mathbf{x}}_b^2}{2} = \frac{m_a + m_b}{2} \dot{\mathbf{R}}^2 + \frac{m_{ab}}{2} \dot{\mathbf{r}}^2, \tag{2.28}$$

where the reduced mass is given by

$$m_{ab} = \frac{m_a m_b}{(m_a + m_b)}. \tag{2.29}$$

Therefore, the Lagrangian in eq. (2.24) can be rewritten according to

$$\mathscr{L} = \frac{m_a + m_b}{2} \dot{\mathbf{R}}^2 + \frac{m_{ab}}{2} \dot{\mathbf{r}}^2 + \frac{Z_0 m_e r_0 c^2}{r}. \tag{2.30}$$

By applying the Euler-Lagrange equations for $\mathbf{R}$, we see that the center of mass vector must move with a constant velocity:

$$\frac{d}{dt} \left(\frac{\partial \mathscr{L}}{\partial \dot{\mathbf{R}}} \right) - \frac{\partial \mathscr{L}}{\partial \mathbf{R}} = 0 \Rightarrow \ddot{\mathbf{R}} = 0. \tag{2.31}$$

The motion of the center of mass therefore does not affect the dynamics of the system, so that the first term in eq. (2.30) can be omitted, and the system is described by one particle with the reduced mass m_{ab} and position vector $\mathbf{r}$ interacting with a stationary charge.

After this observation, the scattering angle θ in the center of mass frame can be calculated. We introduce $\mathbf{u} = \dot{\mathbf{r}}$ for the relative velocity of the particles, according to Figure 2.1.
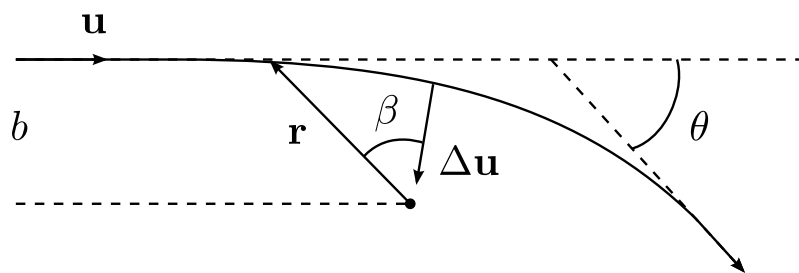
Figure 2.1: The kinematics of a collision. A particle with mass m_{ab} and velocity $\mathbf{u}$ collides with an infinitely heavy particle resulting in a velocity change $\Delta\mathbf{u}$ and a deflection angle θ. The impact parameter b is the minimal distance between the particles without interaction. The two auxiliary variables β and $\mathbf{r}$ are also introduced.

The total change in momentum will then be given by the time integral of the force:

$$m_{ab}\Delta\mathbf{u} = \int_{-\infty}^{\infty} dt \frac{Z_0 m_e r_0 c^2}{r(t)^2} \hat{\mathbf{r}}(t). \tag{2.32}$$

We can now make a few simplifications. Firstly, since the integral is parallel to $\Delta\mathbf{u}$, we can project the vector $\hat{\mathbf{r}}$ in this direction by introducing the angle β between $\Delta\mathbf{u}$ and the relative position $\mathbf{r}$. Secondly, it is useful to observe that the angular momentum is conserved in the collision and can be rewritten using the impact parameter b: $r^2\dot{\beta} = bu$. Equation (2.32) can therefore be rewritten as

$$m_{ab}\Delta u = Z_0 m_e r_0 c^2 \int_{-\infty}^{\infty} dt\, \frac{\dot{\beta}}{bu} \cos\beta. \tag{2.33}$$

The integral can by symmetry be reduced to twice the integral over the interval $t \in (-\infty, 0]$. In rewriting the integral to be over the angle β, the integration limits are obtained geometrically from noting that since the magnitude of the velocity u is the same before and after the collision, $2\beta(t \to -\infty) = \pi + \theta$. By symmetry the relation $\Delta u = 2u\sin(\theta/2)$ is also obtained. This gives

$$m_{ab}2u\sin(\theta/2) = \frac{Z_0 m_e r_0 c^2}{bu} 2 \int_{\beta(t\to-\infty)}^{0} d\beta \cos\beta \tag{2.34}$$

$$\Rightarrow$$

$$\tan(\theta/2) = \frac{Z_0 m_e r_0 c^2}{bu^2 m_{ab}}. \tag{2.35}$$

The final step in obtaining the cross section $d\sigma/d\Omega$ is a change of variables from the impact parameter b to the scattering angle θ. Using eq. (2.35) it is obtained by

$$\frac{d\sigma}{d\Omega} = \frac{b|db|}{\sin\theta d\theta} = \left(\frac{Z_0 r_0 m_e c^2}{2m_{ab}u^2}\right)^2 \frac{1}{\sin^4(\theta/2)}. \tag{2.36}$$

Equation (2.36) can now readily be inserted into the eq. (2.18) and we obtain the Fokker–Planck operator. With this choice of physical constants, the dimension of the cross section as an area is manifest.

2.2.2 Fokker–Planck operator for classical, non-relativistic Coulomb interaction

The Fokker–Planck equation in the case of Coulomb interaction was originally derived by Landau [26]. In this section we follow Rosenbluth et al., who further developed the formalism [27]. Note that Rosenbluth et al. use CGS while this text uses SI units. Another difference to the original paper is that we keep the charges of the colliding species general. We follow the conventions in Helander and Sigmar [2], and therefore some variables appear with different numerical factors compared to the Rosenbluth paper.

Starting from the Fokker–Planck collision operator in eq. (2.18), we first find the velocity changes needed for eqs. (2.19) and (2.20) given the cross section derived in Section 2.2.1. As in the derivation of the Rutherford cross section in Section 2.2.1, the center of mass frame is preferable. With $\mathbf{v}$ and $\mathbf{v}'$ denoting the velocities for

particles a and b, $\mathbf{V}$ for the center of mass velocity and $\mathbf{u} = \mathbf{v} - \mathbf{v}'$ being the relative velocity, these relations follow

$$\mathbf{V} = \frac{m_a}{m_a + m_b}\mathbf{v} + \frac{m_b}{m_a + m_b}\mathbf{v}', \tag{2.37}$$

$$\mathbf{v} = \mathbf{V} + \frac{m_b}{m_a + m_b}\mathbf{u}, \tag{2.38}$$

$$\mathbf{\Delta v} = \frac{m_b}{m_a + m_b}\mathbf{\Delta u}, \tag{2.39}$$

since the center of mass velocity is constant throughout the collision. The problem of finding the change in velocity of particle of type a required in eq. (2.18) is therefore reduced to finding the change in the relative velocity.

In order to determine $\mathbf{\Delta u}$, we proceed as follows. Let $\{\mathbf{e}_i\}$ denote an arbitrary, inertial Cartesian coordinate system, and introduce the local coordinate system with unit vectors $\{\mathbf{e}_{i,L}\}$ aligned with the relative velocity before the collision. $\mathbf{\Delta u}_L$ (in the system $\{\mathbf{e}_{i,L}\}$) is straightforward to calculate, and the results are transformed to the system $\{\mathbf{e}_i\}$ where the integrals in eq. (2.18) are carried out.

The system $\{\mathbf{e}_{i,L}\}$ is described by

$$\mathbf{e}_{1,L} = \frac{\mathbf{u}}{u}, \quad \mathbf{e}_{2,L} = \frac{\mathbf{e}_3 \times \mathbf{u}}{\sqrt{(u^1)^2 + (u^2)^2}}, \quad \mathbf{e}_{3,L} = \mathbf{e}_{1,L} \times \mathbf{e}_{2,L}, \tag{2.40}$$

where the normalization factor in $\mathbf{e}_L^2$ is found for example by writing

$$\mathbf{u} = u^3\mathbf{e}_3 + u^\perp\mathbf{e}_\perp; \quad |\mathbf{e}_3 \times \mathbf{u}| = u^\perp = \sqrt{(u^1)^2 + (u^2)^2}. \tag{2.41}$$

Defining θ to be the deflection angle, and ϕ as the rotation around $\mathbf{u}$, $\mathbf{\Delta u}_L$ is given by

$$\begin{aligned}
\Delta u_L^1 &= u(\cos\theta - 1) = -2u\sin^2(\theta/2), \\
\Delta u_L^2 &= u\sin\theta\cos\phi = 2u\cos(\theta/2)\sin(\theta/2)\cos\phi, \\
\Delta u_L^3 &= u\sin\theta\sin\phi = 2u\cos(\theta/2)\sin(\theta/2)\sin\phi.
\end{aligned} \tag{2.42}$$

We are now at a point where we can integrate over scattering angles to calculate eqs. (2.19) and (2.20). The lowest order terms will however diverge logarithmically. This is solved by considering Debye shielding, see 2.2.3, which in turn leads to a minimum deflection angle (or maximum impact parameter) and therefore a cutoff in the integrals. This cutoff leads to the definition of the Coulomb logarithm $\ln\Lambda$ presented in Section 2.2.3. By only keeping the leading order terms in the Coulomb logarithm, we will see why the first two velocity moments in the Fokker–Planck equation suffice. Let us however start by calculating the required first-order moments.

For simplicity we now define (still in the local coordinate system)

$$\{\Delta u_L^\mu\} = \int d\Omega \frac{d\sigma}{d\Omega} u\Delta u_L^\mu. \tag{2.43}$$

By the properties of trigonometric functions appearing in eq. (2.42) and the cross section in eq. (2.36), the second and third components of $\{\Delta u_L^\mu\}$ vanish, while the

first component is

$$\{\Delta u_L^1\} = \int_0^\pi \sin\theta d\theta \int_0^{2\pi} \left(\frac{Z_0 r_0 m_e c^2}{2 m_{ab} u^2}\right)^2 \frac{1}{\sin^4(\theta/2)} u \left(-2u\sin^2(\theta/2)\right) d\phi$$

$$\approx -4\pi \left(\frac{Z_0 r_0 m_e c^2}{m_{ab} u^2}\right)^2 \int_{\theta_{\min}}^\pi \frac{1}{2}\frac{\cos(\theta/2)}{\sin(\theta/2)}d\theta$$

$$= -\frac{\Gamma_{ab}}{4\pi}\frac{m_a^2}{m_{ab}^2}\frac{1}{u^2}, \tag{2.44}$$

where we introduced the cutoff at $\theta_{\min}$, and made the small angle approximation $\sin\theta_{\min} \approx \theta_{\min}$. The Coulomb logarithm, discussed in Section 2.2.3, is then defined according to

$$\ln\Lambda \equiv \ln\left(\frac{2}{\theta_{\min}}\right). \tag{2.45}$$

For convenience we have also defined

$$\Gamma_{ab} = (4\pi)^2 \left(\frac{m_e}{m_a}Z_0 c^2 r_0\right)^2 \ln\Lambda. \tag{2.46}$$

Continuing with the higher moments, we note that

$$d\Omega\frac{d\sigma}{d\Omega} \propto 2\cos(\theta/2)\sin^{-3}(\theta/2)d\theta d\phi. \tag{2.47}$$

Neglecting terms of order unity in $\ln\Lambda$, only the $\{\Delta u_L^\mu \Delta u_L^\nu\}$ terms with less than three powers of $\sin(\theta/2)$ will contribute. Therefore, from eq. (2.42), the only components of interest are

$$(i)\ \{\Delta u_L^2\ \Delta u_L^2\}, \qquad (ii)\ \{\Delta u_L^3\ \Delta u_L^3\}, \qquad (iii)\ \{\Delta u_L^2\ \Delta u_L^3\}. \tag{2.48}$$

The last term (iii) vanishes by symmetry when integrating over ϕ. Terms of order three and higher will all have at least three powers of $\sin(\theta/2)$ and will therefore contain no powers of the Coulomb logarithm. Thus, the only remaining moments to calculate are

$$\{\Delta u_L^2 \Delta u_L^2\} = \{\Delta u_L^3 \Delta u_L^3\}$$

$$= \left(\frac{Z_0 r_0 m_e c^2}{2 m_{ab} u^2}\right)^2 \cdot 8\pi u^3 \int_0^\pi d\theta \frac{\cos^3(\theta/2)}{\sin(\theta/2)}$$

$$= \frac{1}{u}\left(\frac{Z_0 r_0 m_e c^2}{m_{ab} u^2}\right)^2 \left(\int_{\theta_{\min}}^\pi \frac{1}{2}\frac{\cos(\theta/2)}{\sin(\theta/2)}d\theta + \mathcal{O}\left(\left[\frac{1}{\ln\Lambda}\right]^0\right)\right)$$

$$\approx \frac{\Gamma_{ab}}{4\pi}\frac{m_a^2}{m_{ab}^2}\frac{1}{u}. \tag{2.49}$$

In order to transform back to the absolute velocity in the original coordinate system, use eq. (2.39) and

$$\Delta u^\mu = (\mathbf{e}^\mu \cdot \mathbf{e}_{L,\nu})\Delta u_L^\nu, \tag{2.50}$$

$$\Delta u^\mu \Delta u^\nu = (\mathbf{e}^\mu \cdot \mathbf{e}_{L,\sigma})(\mathbf{e}^\nu \cdot \mathbf{e}_{L,\rho})\Delta u_L^\sigma \Delta u_L^\rho. \tag{2.51}$$

This gives

$$
\begin{aligned}
\{\Delta v^\mu\} =& \frac{m_b}{m_a + m_b}(\mathbf{e}^\mu \cdot \mathbf{e}_{L,1})\{\Delta u_L^1\} \\
&\Rightarrow \left[\mathbf{e}^\mu \cdot \mathbf{e}_{L,1} = \mathbf{e}^\mu \cdot \frac{\mathbf{u}}{u} = \frac{u^\mu}{u}\right] \Rightarrow \\
=& -\frac{u^\mu}{u}\frac{m_b}{m_a + m_b}\frac{\Gamma_{ab}}{4\pi}\frac{m_a^2}{m_{ab}^2}\frac{1}{u^2} \\
=& -\frac{u^\mu}{u^3}\frac{m_a}{m_{ab}}\frac{\Gamma_{ab}}{4\pi},
\end{aligned}
\tag{2.52}
$$

where we used eq. (2.29) for the reduced mass.

To obtain $\{\Delta v^\mu \Delta v^\nu\}$, note that the Kronecker delta can be rewritten as

$$
\delta^{\mu\nu} = \mathbf{e}^\mu \cdot (\mathbf{e}_{L,1}\mathbf{e}_{L,1} + \mathbf{e}_{L,2}\mathbf{e}_{L,2} + \mathbf{e}_{L,3}\mathbf{e}_{L,3}) \cdot \mathbf{e}^\nu.
\tag{2.53}
$$

This gives

$$
\begin{aligned}
\{\Delta v^\mu \Delta v^\nu\} =& \left(\frac{m_b}{m_a + m_b}\right)^2 \Big[(\mathbf{e}^\mu \cdot \mathbf{e}_{L,2})(\mathbf{e}^\nu \cdot \mathbf{e}_{L,2})+ \\
&+ (\mathbf{e}^\mu \cdot \mathbf{e}_{L,3})(\mathbf{e}^\nu \cdot \mathbf{e}_{L,3})\Big]\{\Delta u_L^2 \Delta u_L^2\} \\
=& \left(\frac{m_b}{m_a + m_b}\right)^2 [\delta^{\mu\nu} - (\mathbf{e}^\mu \cdot \mathbf{e}_{L,1})(\mathbf{e}^\nu \cdot \mathbf{e}_{L,1})]\frac{\Gamma_{ab}}{4\pi}\frac{m_a^2}{m_{ab}^2}\frac{1}{u} \\
=& \frac{1}{u}\left[\delta^{\mu\nu} - \frac{u^\mu u^\nu}{u^2}\right]\frac{\Gamma_{ab}}{4\pi}.
\end{aligned}
\tag{2.54}
$$

A further simplification is possible noting that

$$
u = \sqrt{(v^\mu - v'^\mu)^2} \Rightarrow \nabla_{\mathbf{v}}^\mu u = \frac{u^\mu}{u},
\tag{2.55}
$$

$$
\nabla_{\mathbf{v}}^\mu \frac{1}{u} = -\frac{u^\mu}{u^3},
\tag{2.56}
$$

$$
\nabla_{\mathbf{v}}^\mu \nabla_{\mathbf{v}}^\nu u = \frac{1}{u}\left(\delta^{\mu\nu} - \frac{u^\mu u^\nu}{u^2}\right).
\tag{2.57}
$$

The upper index on the differential operators are used to be consistent with covariant notation used in Chapters 3 and 4.

We thus end up with the following two expressions ready to use in the final expression for the Fokker-Planck operator:

$$
\{\Delta v^\mu\} = \Gamma_{ab}\frac{m_a}{m_{ab}}\nabla^\mu \frac{1}{u},
\tag{2.58}
$$

$$
\{\Delta v^\mu \Delta v^\nu\} = \Gamma_{ab}\nabla^\mu \nabla^\nu u.
\tag{2.59}
$$

From eq. (2.19) and (2.20), we then get

$$
\begin{aligned}
\langle \Delta v^{\mu} \rangle_a &= \sum_b \int d\mathbf{v}' f_b(\mathbf{v}') \{\Delta v^{\mu}\} \\
&= \sum_b \frac{\Gamma_{ab}}{4\pi} \frac{m_a}{m_{ab}} \int d\mathbf{v}' f_b(\mathbf{v}') \nabla^{\mu} \frac{1}{u} \\
&= \nabla^{\mu} \sum_b \frac{\Gamma_{ab}}{4\pi} \frac{m_a}{m_{ab}} \int d\mathbf{v}' f_b(\mathbf{v}') \frac{1}{|\mathbf{v} - \mathbf{v}'|},
\end{aligned}
\tag{2.60}
$$

and

$$
\begin{aligned}
\langle \Delta v^{\mu} \Delta v^{\nu} \rangle_a &= \sum_b \int d\mathbf{v}' f_b(\mathbf{v}') \{\Delta v^{\mu} \Delta v^{\nu}\} \\
&= \nabla^{\mu} \nabla^{\nu} \sum_b \frac{\Gamma_{ab}}{4\pi} \int d\mathbf{v}' f_b(\mathbf{v}') |\mathbf{v} - \mathbf{v}'|.
\end{aligned}
\tag{2.61}
$$

The final step of re-writing these equations is to use the elegant and convenient Rosenbluth potentials,

$$
\varphi_b(u) \equiv -\frac{1}{4\pi} \int d\mathbf{v}' f_b(\mathbf{v}') \frac{1}{|\mathbf{v} - \mathbf{v}'|},
\tag{2.62}
$$

$$
\psi_b(u) \equiv -\frac{1}{8\pi} \int d\mathbf{v}' f_b(\mathbf{v}') |\mathbf{v} - \mathbf{v}'|.
\tag{2.63}
$$

The name originates from the similarities with potential theory; the relation between φ_b and the distribution function f_b is similar to the relationship between, for example, the electromagnetic scalar potential and the charge density. Using the Rosenbluth potentials, we may rewrite

$$
\langle \Delta v^{\mu} \rangle_a = -\nabla^{\mu} \sum_b \Gamma_{ab} \frac{m_a}{m_{ab}} \varphi_b,
\tag{2.64}
$$

$$
\langle \Delta v^{\mu} \Delta v^{\nu} \rangle_a = -2\nabla^{\mu} \nabla^{\nu} \sum_b \Gamma_{ab} \psi_b.
\tag{2.65}
$$

This yields for the Fokker–Planck eq. (2.18)

$$
\left(\frac{\partial f_a}{\partial t} \right)_c = \sum_b \Gamma_{ab} \left[\frac{m_a}{m_{ab}} \nabla_{\mu} \left(f_a \nabla^{\mu} \varphi_b \right) - \nabla_{\mu} \nabla_{\nu} \left(f_a \nabla^{\mu} \nabla^{\nu} \psi_b \right) \right].
\tag{2.66}
$$

To highlight the physical properties of the collision operator, we note that the Rosenbluth potentials are related by

$$
\varphi_b \equiv \nabla_{\nu} \nabla^{\nu} \psi_b,
\tag{2.67}
$$

which leads to a partial cancellation between the two terms in eq. (2.66):

$$
\left(\frac{\partial f_a}{\partial t} \right)_c = \sum_b \Gamma_{ab} \nabla_{\mu} \left[\frac{m_a}{m_b} f_a \nabla^{\mu} \varphi_b - \nabla_{\nu}(f_a) \nabla^{\mu} \nabla^{\nu} \psi_b \right].
\tag{2.68}
$$

There are a few properties of the collision operator that we would like to emphasize. Firstly, the equilibrium distribution is – inherently from the null space of the Boltzmann operator in Section 2.1.1 – a Maxwellian (see eq. (2.75)). Secondly, the Fokker–Planck collision operator conserves number density of each species, as well as momentum and energy, when considering both species a and b. This is manifested by the following moments:

$$\int d\mathbf{v} \, C^{ab}(f_a) = 0, \tag{2.69}$$

$$\int d\mathbf{v} \, m_a \mathbf{v} C^{ab}(f_a) = -\int d\mathbf{v} \, m_b \mathbf{v} C_{ba}(f_b), \tag{2.70}$$

$$\int d\mathbf{v} \, m_a v^2 C^{ab}(f_a) = -\int d\mathbf{v} \, m_b v^2 C_{ba}(f_b), \tag{2.71}$$

where the total collision operator is the sum over all species b:

$$\left(\frac{\partial f_a}{\partial t}\right)_c = \sum_b C^{ab}. \tag{2.72}$$

2.2.3 Debye shielding and the Coulomb logarithm

The Coulomb logarithm is the standard plasma physics measure of how effectively the long range Coulomb interaction is screened and how dominant the small angle collisions are. The basic idea is that Debye shielding [1] provides the typical length scale of an average collisional interaction, which can be used to determine the typical deflection angle θ in eq. (2.35) for a particle at the thermal velocity.

Although the Coulomb force has an infinite range, a charged particle in a plasma will only interact with its close neighbors. This is due to Debye shielding; upon interacting with other charged particles, a configuration that is neutral when observed from large distances will be achieved. In other words, the plasma is quasineutral, as noted in the Introduction. The Debye length is the length scale over which a charged particle will be "seen" by other particles, before the shielding is strong enough,

$$\lambda_D = \sqrt{\frac{\epsilon_0 T}{ne^2}}, \tag{2.73}$$

where T is the temperature (with the Boltzmann constant k_B set to unity) and n is the number density.

If λ_D provides the maximum impact parameter in a collision, then the minimum deflection angle in eq. (2.35) will be given by

$$\theta_{\min} \approx Z_0 \frac{r_0 c^2}{\lambda_D v_{Ta}^2}, \tag{2.74}$$

where we have approximated the velocity by the thermal velocity and considered the case of electron-ion collisions.

The Coulomb logarithm $\ln \Lambda$ is then defined as the logarithm of this minimum angle inverted[2] and provides a quantification of how dominant small-angle collisions are.

---

[2]Note that in Section 2.2.2 and eq. (2.45), $\ln \Lambda$ differs by $\ln 2$; in this context it is a small difference.

The density and temperature dependence of the Coulomb logarithm shows that the larger the temperature and the lower the density, the higher the Coulomb logarithm. For a typical magnetic fusion plasma, the Coulomb logarithm is of the order 10-20. In cases where $\ln \Lambda \lesssim 10$, the Fokker–Planck treatment is strictly not valid, since large-angle collisions will be important. The reason is that with a small Coulomb logarithm, the higher order terms in the small-angle expansion of the Boltzmann operator as treated in Section 2.1.2 will not be suppressed sufficiently to be neglected.

2.2.4 Collisions with a Maxwellian background: collision frequencies and runaway electrons

The collision operator in eq. (2.66) can be calculated explicitly in a straightforward manner for collisions between a species and a Maxwellian distribution:

$$f_{M,a}(\mathbf{x},\mathbf{t}) = n_a(\mathbf{x},t) \left(\frac{m_a}{2\pi T_a(\mathbf{x},t)} \right)^{3/2} \exp \left(-\frac{m_a[\mathbf{v} - \mathbf{V}_a(\mathbf{x},t)]^2}{2T_a(\mathbf{x},t)} \right), \qquad (2.75)$$

where n_a is the number density of species a, m_a is its mass, T_a is its temperature and $\mathbf{V}_a$ is the mean flow velocity.

The collision operator for interactions between species a and b can then be written in the following form, and three basic collision frequencies defined

$$C^{ab} = \nu_D^{ab}\mathscr{L}(f_a) + \frac{1}{v^2}\frac{\partial}{\partial v}\left[v^3 \left(\nu_S^{ab} f_a + \frac{1}{2}\nu_\parallel^{ab} v \frac{\partial f_a}{\partial v} \right) \right]. \qquad (2.76)$$

The Lorentz scattering operator is proportional to the angular part of the divergence operator:

$$\mathscr{L} = \frac{1}{2}\left[\frac{1}{\sin\theta}\frac{\partial}{\partial\theta}\left(\sin\theta \frac{\partial}{\partial\theta} \right) + \frac{1}{\sin^2\theta}\frac{\partial^2}{\partial\phi^2} \right]. \qquad (2.77)$$

In case of azimuthal symmetry with $\xi = \cos\theta$, the Lorentz scattering operator can be simplified to

$$\mathscr{L} = \frac{1}{2}\frac{\partial}{\partial\xi}\left(1 - \xi^2 \right)\frac{\partial}{\partial\xi}. \qquad (2.78)$$

The collision frequencies in eq. (2.76) describe three fundamental processes. The deflection frequency ν_D^{ab} describes diffusion at constant energy (also called pitch-angle scattering), and the parallel velocity diffusion frequency $\nu_\parallel^{ab}$ is associated with diffusion of the absolute particle velocity. The slowing-down frequency ν_S^{ab} is associated with the piece of the collision operator which acts like a typical frictional force. Note that we define ν_S^{ab} differently from Helander and Sigmar [2], without the mass ratio $m_a/(m_a + m_b)$. This is done for clarity when the screening corrections are considered in Chapters 3 and 4.

The collision frequencies are

$$\nu_D^{ab} = \hat{\nu}_{ab} \frac{\phi(x_b) - G(x_b)}{x_a^3}, \tag{2.79}$$

$$\nu_S^{ab} = \hat{\nu}_{ab} \frac{2T_a}{T_b} \frac{G(x_b)}{x_a}, \tag{2.80}$$

$$\nu_\parallel^{ab} = 2\hat{\nu}_{ab} \frac{G(x_b)}{x_a^3}, \tag{2.81}$$

$$\hat{\nu}_{ab} = \frac{n_b}{v_{Ta}^3} \frac{\Gamma_{ab}}{4\pi}, \tag{2.82}$$

where $x_a = v/v_{Ta}$ is the normalized velocity, $v_{Ta} = \sqrt{2T_a/m_a}$ is the thermal speed,

$$\phi(x) = \frac{2}{\sqrt{\pi}} \int_0^x e^{-y^2} dy \tag{2.83}$$

is the error function, and

$$G(x) = \frac{\phi(x) - x\phi(x)}{2x^2} \to \begin{cases} \frac{2x}{3\sqrt{\pi}}, & x \to 0 \\ \frac{1}{2x^2}, & x \to \infty \end{cases} \tag{2.84}$$

is the Chandrasekhar function which is plotted in Figure 2.2.
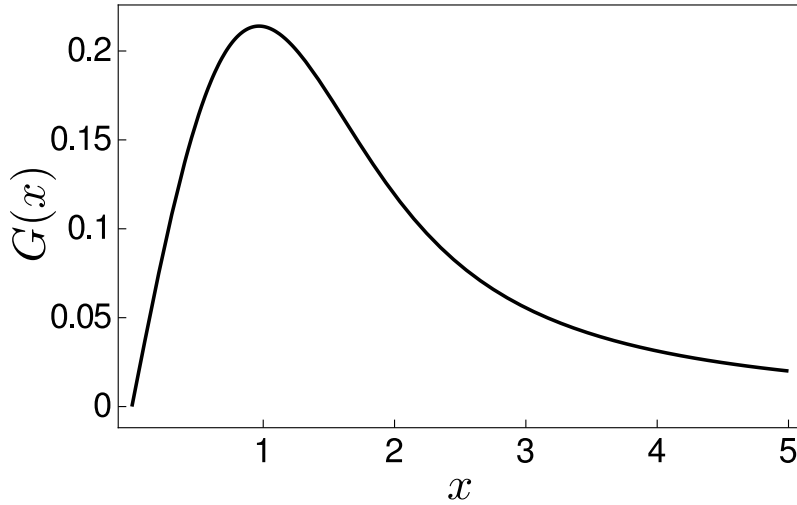
Figure 2.2: The Chandrasekhar function naturally appears in the collision frequencies for a Maxwellian background distribution. It decreases for large arguments, leading to a decreasing drag force with velocity.

Later in this report we study the special case where $v/v_{Tb} \gg 1$. We then take $x_b \to \infty, \phi(x) \to 1$. This gives the collision frequencies for collisions with stationary particles b. In this limit we get

$$\nu_D^{ab} \to n_b \frac{\Gamma_{ab}}{4\pi} \frac{1}{v^3}, \tag{2.85}$$

$$\nu_S^{ab} \to n_b \left(\frac{m_a}{m_b}\right) \frac{\Gamma_{ab}}{4\pi} \frac{1}{v^3}, \tag{2.86}$$

$$\nu_\parallel^{ab} \to 0, \tag{2.87}$$

where Γ_{ab} is defined in eq. (2.46).

The fundamental mechanism for creation of runaway electrons, as discussed in the Introduction, can be seen from the behavior of ν_S^{ab} in eq. (2.80). The friction force on a particle of species a due to collisions with particles of species b is proportional to the average change of the velocity per unit time,

$$F = m_a \langle v_\parallel \rangle^{ab} \sim -m_a v_\parallel \nu_S^{ab} \propto G(x_b). \tag{2.88}$$

For large velocities, the Chandrasekhar function (Figure 2.2) decreases with increasing velocity. If an electric field is applied, it will cause the fastest particles in the tail of the velocity distribution to accelerate and "run away". The scale of the electric fields needed are described by the Dreicer field and the critical field [2]. The Drecier field sets the scale at which the bulk population runs away,

$$E_D = \frac{n_e e^3 \ln \Lambda}{4\pi \epsilon_0^2 T_e}, \tag{2.89}$$

while the critical field

$$E_c = \frac{n_e e^3 \ln \Lambda}{4\pi \epsilon_0^2 m_e c^2} \tag{2.90}$$

is the minimal field that must be exceeded to produce runaways at all as noted in the Introduction. The critical field arises from relativistic considerations in the high-momentum limit of the friction force on a fast electron [11].

2.3 Quantum mechanical effects on cross sections

For collisional interactions mediated by the Coulomb force between an ion and a low-momentum particle, the distance of closest approach will be much larger than the spatial scale of the ion. The particle will then be unaffected by the internal structure of the target. A good approximation is therefore to assume complete screening meaning that the particle experiences the interaction due only to the actual charge state of the ion. On the other hand, a particle with high momentum can penetrate the electron cloud surrounding the nucleus and the fully screened approximation no longer holds. A quantum mechanical approach is needed to achieve a more accurate description of such collision dynamics, as the de Broglie wavelength of runaway electrons is small compared to the ion size.

Compared to collisions with a fully ionized ion, a particle interacting with a partially ionized ion will experience a change in the cross section of elastic scattering, which is complemented by the possibility of inelastic collisions with the bound electrons of the ion. Both these contributions may enhance the collision rates experienced by the particle compared to the assumption of full screening. Inelastic collisions are not considered in this thesis but would be needed for a complete description of collisions with partially ionized ions.

This section presents the quantum mechanical scattering cross section for elastic collisions and discusses the two limits of small and large incoming particle momentum.

This cross section can then be used to obtain a Fokker–Planck collision operator that accounts for screening effects, which is done in Chapters 3 and 4.

2.3.1 Scattering cross section

The scattering cross section takes an elegant form in the Born approximation. In this leading-order perturbation model, it is assumed that the wavefunction of the scattered particle is only altered slightly by the scattering potential and can thus be approximated by a free-particle incoming wave [28]. In the Born approximation, the cross section for elastic scattering of a fast electron by an ion is [22]

$$\frac{d\sigma}{d\Omega} = \frac{1}{4}\left(\frac{m_e}{m_{ab}}\frac{r_0 c^2}{u^2}\right)^2 \frac{[Z - F(q)]^2}{\sin^4(\theta/2)}, \tag{2.91}$$

where

$$q = \frac{2m_{ab}u}{\hbar}\sin(\theta/2), \tag{2.92}$$

and the classical electron radius r_0 is given by eq. (2.25). The atomic form factor $F(q)$ is the Fourier transform of the electron density around the ion and is given by

$$F(q) = \int d\mathbf{r}\, n_e(r) e^{-i\mathbf{q}\cdot\mathbf{r}}. \tag{2.93}$$

With relativistic corrections, the scattering cross section acquires an extra factor of $(\cos^2(\theta/2)k^2 + 1)$, where $k = p/(m_e c)$ is the normalized momentum. In Chapter 4, the relativistic case will be treated in the limit of zero mass ratio m_a/m_b. In this limit, the relativistic scattering cross section is given in the standard textbook [29]:

$$\frac{d\sigma}{d\Omega} = \frac{r_0^2}{4}\frac{[Z - F(q)]^2}{\sin^4(\theta/2)}\frac{1}{k^4}\left(\cos^2(\theta/2)k^2 + 1\right), \tag{2.94}$$

where $q = 2\sin(\theta/2)p/\hbar$.

2.3.2 Limiting values of the form factor

The high and low momentum limits of the form factor confirm the intuitive picture that a low energy particle will experience full screening, while a high energy particle will interact with the bare nucleus charge. The following argument is a modified version of that in Landau and Lifshitz [22].

Firstly, for low momentum, a power series expansion in q of the form factor in eq. (2.93) gives, to leading order

$$F(\mathbf{q}) = \int d\mathbf{r}\, n_e(r) + \mathcal{O}(qa) = N_e + \mathcal{O}(qa). \tag{2.95}$$

Here N_e is the number of bound electrons and a is the assumed length scale of the atom. In the low energy limit,

$$Z - F \to Z - N_e \equiv Z_0, \tag{2.96}$$

where Z_0 is the net charge state of the ion.

Turning to the high energy limit, the exponential factor in eq. (2.93) will be rapidly oscillating, and the total form factor should therefore be small:

$$Z - F \to Z \equiv X Z_0, \tag{2.97}$$

where $X = Z/Z_0$ is the inverse ionization degree.

Consequently, the high energy cross section will be enhanced by a factor of X^2 compared to the completely screened case. This means that in some cases the dynamics of collisional scattering is expected to be strongly affected by this more accurate treatment of collisions, as discussed in the Introduction. This possibility is considered in Chapters 3 and 4. The two limits of the form factor presented are useful to validate the full momentum-dependence of the cross section, but are also useful to roughly determine the energy-dependence of the form factor, which is done in Section 3.3.4.

3

Non-Relativistic Screened Collision Operator

An accurate description of screening is expected to have a large impact on the collision operator, as noted in Section 2.3.2. For example in the case of singly ionized argon, the collision rates will be enhanced by a factor of the order $X^2 = Z^2 \sim 300$ when comparing total penetration to full screening. The factor of X is here the inverse ionization degree, as defined in eq. (2.97). Whether the colliding particle is screened or penetrates the ion will depend on its momentum through the form factor, which was described in Section 2.3.2. To account for screening at low, non-relativistic energies, the terms in the Fokker Planck collision operator are computed here including the quantum mechanical effects through the form factor. This demonstrates the method to be used in the relativistic calculation in Chapter 4.

In this chapter, we derive general equations for the collision operator when the effect of screened nuclei is taken into account. We follow the main steps of Rosenbluth et al. [13] but replace the fully screened cross section with the quantum mechanical cross section. In addition, we consider terms of higher order in the Taylor expanded Boltzmann operator. As in earlier works where the quantum mechanical effect on the cross section is treated (Refs. [18, 20]; results used by Refs [17, 19]), we use the form factor to model the screening effects. Our derivation is independent from these works, and we we explore various alternative models of the bound electron density. The validity of the Fokker–Planck treatment, as well as the sensitivity to the chosen bound electron density, which were not considered in previous works, are addressed.

3.1 General equations

In this section, we derive the terms in the Fokker–Planck operator using an arbitrary form factor in the quantum mechanical cross section of Section 2.3.1. A complication that comes with the possible large enhancement of the cross section for energetic particles (see Section 2.3.2) is that the standard plasma physics approach of only retaining the leading order terms in $\ln \Lambda$ must be tested. This is because the Coulomb logarithm is not the only large number present for partially ionized ions: there is also the inverse ionization degree X. In this section, we therefore derive the formulas for the small-angle expansion of the Boltzmann collision operator for terms of arbitrary order, of which the first two orders give the Fokker-Planck operator in

eq. (2.18). This allows us to investigate under what conditions the Fokker–Planck approximation is still valid, which we address by comparing the size of higher order terms of the expanded Boltzmann operator in Section 3.3.2.

The Fokker–Planck operator from eq. (2.18) is easily converted to the Taylor expanded form of the Boltzmann operator by including terms of higher order:

$$\left(\frac{\partial f_a}{\partial t}\right)_c = \sum_{k=1}^{\infty} \frac{(-1)^k}{k!} \nabla_{\mu_1} \cdots \nabla_{\mu_k} \left(f_a \langle \Delta v^{\mu_1} \cdots \Delta v^{\mu_k} \rangle_a \right). \tag{3.1}$$

Adapting the formalism from Section 2.2.2 we have

$$\langle \Delta v^{\mu_1} \cdots \Delta v^{\mu_k} \rangle_a = \sum_b \int d\mathbf{v}' f_b(\mathbf{v}') \{\Delta v^{\mu_1} \cdots \Delta v^{\mu_k}\}, \tag{3.2}$$

where the change in the incoming velocity $\mathbf{v}$ of species a is related to the change of the relative velocity u of the particles by

$$\left(1 + \frac{m_a}{m_b}\right)^k \{\Delta v^{\mu_1} \cdots \Delta v^{\mu_k}\} = \{\Delta u^{\mu_1} \cdots \Delta u^{\mu_k}\} = \int d\Omega \frac{d\sigma}{d\Omega} u \Delta u^{\mu_1} \cdots \Delta u^{\mu_k}. \tag{3.3}$$

The changes in relative velocity components in the local frame are

$$\begin{aligned}
\Delta u_L^1 &= u(\cos\theta - 1) = -2u\sin^2(\theta/2), \\
\Delta u_L^2 &= u\sin\theta\cos\phi = 2u\cos(\theta/2)\sin(\theta/2)\cos\phi, \\
\Delta u_L^3 &= u\sin\theta\sin\phi = 2u\cos(\theta/2)\sin(\theta/2)\sin\phi.
\end{aligned} \tag{3.4}$$

From Section 2.3.1 and eq. (2.91), the cross section for collisions between a particle of charge e and an ion with atomic number Z having N_e bound electrons, can be written

$$d\Omega \frac{d\sigma}{d\Omega} = \frac{1}{2} \left(\frac{m_e}{m_{ab}} \frac{r_0 c^2}{u^2}\right)^2 \frac{\cos(\theta/2)}{\sin^3(\theta/2)} \left[Z - F\left(\frac{y}{a}\sin[\theta/2]\right) \right]^2 d\theta d\phi, \tag{3.5}$$

where $r_0 = \alpha^2 a_0$ is the classical electron radius, $\alpha \approx 1/137$ is the fine-structure constant, $a_0 = \hbar/(m_e c \alpha)$ is the Bohr radius. The typical length scale, a, of the atom is introduced so that y can be defined as a dimensionless quantity proportional to momentum:

$$y = \frac{2a m_{ab} u}{\hbar} \equiv \frac{a}{a_0} \frac{m_{ab}}{m_e} \frac{2k}{\alpha}, \tag{3.6}$$

where we have defined the normalized momentum $k = p/(m_e c)$. In the non-relativistic limit, $k = u/c$; when we later consider the relativistic case in Chapter 4 we have $k = \gamma u/c$. We will see that y and k will be key parameters of our results. Note that if electron-ion collisions are considered, $m_{ab} \approx m_e$ since the ions are much heavier than the electrons; additionally we may approximate the ionic length scale by $a \sim a_0$ and therefore $y \sim 2k/\alpha \approx 274k$ for electron-ion collisions.

To get an expression for the moments in eq. (3.3), we first consider the integral over the azimuthal angle, from which we can find which moments vanish by symmetry.

There are three possible types of term: those in which $\cos\phi$ and $\sin\phi$ are both raised to even powers, or both are raised to odd powers, or those in which one in raised to an odd power and the other even:

$$\int_0^{2\pi} d\phi \sin^{2n}\phi \cos^{2m}\phi = 2\frac{\Gamma(\frac{1}{2}+m)\Gamma(\frac{1}{2}+n)}{\Gamma(1+m+n)} \equiv A_{nm}, \qquad (3.7)$$

$$\int_0^{2\pi} d\phi \sin^{2n+1}\phi \cos^{2m+1}\phi = 0, \qquad (3.8)$$

$$\int_0^{2\pi} d\phi \sin^{2n+1}\phi \cos^{2m}\phi = 0. \qquad (3.9)$$

A_{mn} has the property that it is symmetric, $A_{mn} = A_{nm}$, and the first terms are

$$A_{00} = 2\pi, \qquad (3.10)$$
$$A_{10} = \pi. \qquad (3.11)$$

For a general term $\{\Delta u_L^{\mu_1} \cdots \Delta u_L^{\mu_k}\}$ the possible non-zero terms therefore have the form

$$\{(\Delta u_L^1)^l (\Delta u_L^2)^{2n} (\Delta u_L^3)^{2m}\}, \quad l,n,m \in \mathbb{N}, \qquad (3.12)$$

where $s = l + 2n + 2m$ is the order of the term.

We can now rewrite the general terms in eq. (3.3) in the following form:

$$\{(\Delta u_L^1)^l (\Delta u_L^2)^{2n} (\Delta u_L^3)^{2m}\} = (-1)^l 2^s \left(\frac{m_e}{m_{ab}} r_0 c^2\right)^2 \frac{A_{mn}}{u^{3-s}}$$

$$\times \int_{\theta_{\min}}^{\pi} d\theta \frac{\left(\cos(\theta/2)\right)^{1+2n+2m}}{\left(\sin(\theta/2)\right)^{3-s-l}} \left[Z - F\left(\frac{y}{a}\sin[\theta/2]\right)\right]^2$$

$$= \left[\begin{array}{c} x = \sin(\theta/2) \quad 2dx = \cos(\theta/2)d\theta \\ \theta \in [\theta_{\min}, \pi] \Rightarrow x \in \left[\frac{\theta_{\min}}{2}, 1\right] \end{array}\right]$$

$$= (-1)^l 2^s \left(\frac{m_e}{m_{ab}} r_0 c^2\right)^2 \frac{A_{mn}}{u^{3-s}} I_{lmn}(u), \qquad (3.13)$$

where $I_{lmn}(u)$ denotes the integral

$$I_{lmn}(u) \equiv \int_{\theta_{\min}/2}^1 dx \frac{(1-x^2)^{m+n}}{x^{3-s-l}} \left[Z - F\left(\frac{y}{a}x\right)\right]^2. \qquad (3.14)$$

For the standard, fully screened Fokker-Planck collision operator ($Z - F \to Z - N_e$), the terms with the Coulomb logarithm $\ln\Lambda$, see Section 2.2.3, will dominate; these are the terms that diverge as $\theta_{\min} \to 0$. From eq. (3.14) the terms are

$$s + l \leq 2 \Rightarrow (s,l) = \left\{(1,1), (2,0)\right\} \Rightarrow \left\{\{(\Delta u_L^1)\}, \{(\Delta u^2)_L^2\} = \{(\Delta u_L^3)^2\}\right\}, \quad (3.15)$$

as we saw in Section 2.2.2. The same behavior is expected in the limits of low and high momentum when screening is accounted for; in these limits the form factor is

constant as discussed in Section 2.3.2, and once again terms smaller by a factor of $1/\ln\Lambda$ can be neglected.

In the region of intermediate momentum however, some terms in eq. (3.14) may reach their high-momentum limits more rapidly than others. As an upper limit on how large the rapidly increasing terms are compared to the slowly increasing terms, we study the low and high momentum limits of the form factor; $Z - F(q) \to Z_0$ when the nucleus is fully screened and $Z - F(q) \to XZ_0$ in the case of full ion penetration, see eqs. (2.96) and (2.97). The relative enhancement of the terms will therefore be bounded by the ratio

$$\frac{[Z - F(q)]^2_{\max}}{[Z - F(q)]^2_{\min}} = X^2.$$ (3.16)

For a partially ionized heavy ion the inverse ionization degree squared, X^2, can be significantly larger than $\ln\Lambda$. To test whether it is still valid to include only the lowest terms in the collision operator (i.e., to use the Fokker–Planck operator as opposed to the Boltzmann operator), it must be checked that there are no terms that approach the high momentum limit significantly faster than others – these terms could acquire a factor of X^2 before the others grow significantly. If there are such terms, it would not be valid to simply neglect all terms that are smaller by a factor of the Coulomb logarithm. These issues will be addressed in Section 3.3.2.

3.2 Yukawa model

When the moments $\{\Delta u^{\mu_1} \cdots \Delta u^{\mu_k}\}$ of the cross section are known, there are just a few more steps to obtain the collision operator. But in order to evaluate these moments, an expression for the form factor is needed, which requires knowledge of the electron density of the ion. There are a few different models at hand, but as will be noted later there are indications that we can capture the necessary physics for the collision operator and also obtain analytical results by using the simple Yukawa potential for the bound electron density, which is sometimes used to model electromagnetic interaction with finite range by equipping the photon with a mass.

The main purpose of the form factor is in our case to provide a transition between the high and low momentum regions. The asymptotic behaviors to match are (see Section 2.3.2)

$$F \to N_e \text{ for } q \ll 1/a; \quad F \to 0 \text{ for } q \gg 1/a,$$ (3.17)

where a is a characteristic length scale of the atom, i.e. of the order of the Bohr radius a_0, which is the most probable distance between the electron and the proton in a ground state hydrogen atom.

A simple model that captures these features with no other free parameters than the length scale is obtained by letting the bound electron density take the same structure as the Yukawa potential,

$$n(\mathbf{r}) = N_e \frac{e^{-r/a}}{4\pi r a^2},$$ (3.18)

where the total number of electrons $N_e = \int n(\mathbf{r})$, and $a \sim a_0$, the Bohr radius.

The form factor is then the Fourier transform:

$$F(\mathbf{q}) = F(q) = \frac{N_e}{a^2 q^2 + 1} = \frac{N_e}{y^2 x^2 + 1}, \quad (3.19)$$

where $x = \sin(\theta/2)$ and y in eq. (3.6) is proportional to the normalized momentum $k = u/c$

$$y = \frac{a}{a_0} \frac{m_{ab}}{m_e} \frac{2k}{\alpha}. \quad (3.20)$$

The resulting cross section (see eq. (2.91)) is shown together with the limiting behavior at low and high momentum in Figure 3.1. In the region close to the transition at $q \sim 1/a$ from the low-momentum behavior to the high-momentum behavior, the q^{-4} power law changes to a slower fall-off, which is manifested by a flatter slope compared to in the two other regions. When integrating the cross section over angles to form I_{lmn} in eq (3.14), the momentum will affect the integration limits in terms of q, since $qa = y\sin(\theta/2)$. This will determine the amount of screening: at low momentum, the integral covers mainly the region before the transition and therefore the fully screened case is obtained; at very high momentum, the region after the transition will dominate the integral leading to no screening; and at intermediate momentum the transition region will be important and we may expect small-angle collisions to be less dominant than at low and high momentum. This is discussed further when higher order terms in the Fokker–Planck operator are considered in Section 3.3.2.
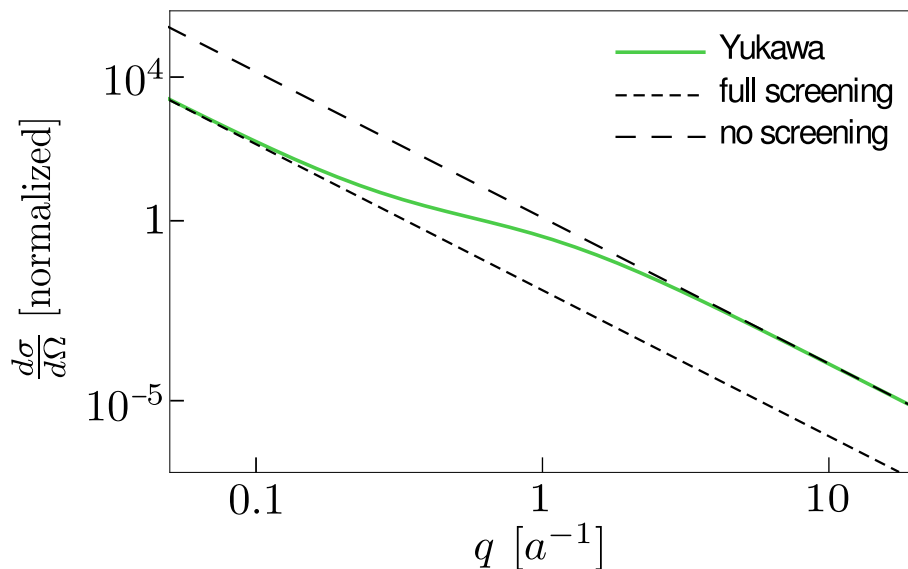
Figure 3.1: The shape of the cross section highlighted on a log-log scale using a Yukawa potential model (solid green), which provides a smooth transition from full screening (dashed black line) to the larger cross section with no screening (long dashed black line). The cross section falls off as $q^4 = [\sin(\theta/2)y/a]^4$, where y is a dimensionless momentum parameter, a is a length scale of the ion and θ is the deflection angle. However the curve is flatter in the transition region around $q \sim 1/a$.

With this simple model for the form factor, we can integrate eq. (3.13) analytically. As

$$\Lambda = \frac{2}{\theta_{\min}} \sim 10^8 \gg 1, \tag{3.21}$$

there will only be a minimal error introduced by neglecting terms of order $\mathcal{O}(\theta_{\min}^1)$. Furthermore, terms of order $y\Lambda^{-1}$, which also arise in eq. (3.13), can also be neglected since the present treatment is non-relativistic in which case (using $m_{ab}a \sim m_e a_0$)

$$y \sim \frac{2}{\alpha} \frac{u}{c} \lesssim 10^2 \ll \Lambda. \tag{3.22}$$

It is therefore reasonable to neglect these terms. In contrast, neglecting terms of order $y\Lambda^{-1}$ changes the behavior of the expressions as $y \to \infty$. These factors must therefore be restored to check the limits (full screening and complete penetration in the high and low momentum limits respectively) in Section 3.3.1.

It is convenient to give the results in terms of the fully screened charge Z_0 and the ionization parameter X according to

$$Z_0 = Z - N_e, \quad X = Z/Z_0. \tag{3.23}$$

Since our partially screened corrections to the fully screened case are of order $1/\ln\Lambda$, we keep all non-zero terms up to second order in the Fokker–Planck equation. Consequently we have three terms ($\{\Delta u_L^1\}$, $\{\Delta u_L^2\Delta u_L^2\}$ and $\{\Delta u_L^1\Delta u_L^1\}$) in contrast to the fully screened case where only $\{\Delta u_L^1\}$, $\{\Delta u_L^2\Delta u_L^2\}$ are non-zero to leading order in the Coulomb logarithm, see Section 2.2.2. The relative size of higher order terms in the Taylor expanded Boltzmann operator is discussed in Section 3.3.2.

To obtain the absolute velocity change, we multiply by the mass ratio according to eq. (3.3) and insert into eq. (3.13). This gives

$$\{\Delta v_L^1\} = \left(\frac{m_b}{m_a + m_b}\right)\{\Delta u_L^1\}$$

$$= -2\left(\frac{m_b}{m_a + m_b}\right)\left(\frac{m_e}{m_{ab}}r_0 c^2\right)^2 \frac{A_{00}}{u^2}I_{100} \tag{3.24}$$

$$= -\frac{\Gamma_{ab}}{4\pi}\left(1 + \frac{m_a}{m_b}\right)\frac{1}{u^2}\left(1 + \frac{g(y)}{\ln\Lambda}\right), \tag{3.25}$$

$$\{\Delta v_L^2\Delta v_L^2\} = \{\Delta v_L^3\Delta v_L^3\} = \left(\frac{m_b}{m_a + m_b}\right)^2\{\Delta u_L^2\Delta u_L^2\}$$

$$= \left(\frac{m_e}{m_a}r_0 c^2\right)^2 \frac{4A_{10}}{u}I_{010}$$

$$= \frac{\Gamma_{ab}}{4\pi}\frac{1}{u}\left(1 + \frac{h(y)}{\ln\Lambda}\right), \tag{3.26}$$

$$\{\Delta v_L^1\Delta v_L^1\} = \left(\frac{m_b}{m_a + m_b}\right)^2\{\Delta u_L^1\Delta u_L^1\}$$

$$= \left(\frac{m_e}{m_a}r_0 c^2\right)^2 \frac{4A_{00}}{u}I_{200}$$

$$= \frac{\Gamma_{ab}}{4\pi}\frac{1}{u}\frac{l(y)}{\ln\Lambda}, \tag{3.27}$$

where $h(y) = g(y) - l(y)/2$ since $I_{010} = I_{100} - I_{200}$ from eq. (3.14)

$$g(y) = \frac{1}{2}\left(X^2 - 1\right)\ln(y^2 + 1) - (X - 1)^2\frac{y^2}{2(y^2 + 1)}, \tag{3.28}$$

$$h(y) = -X(X - 1) + \frac{(X - 1)}{2}\left[\frac{X(y^2 + 2)}{y^2} + 1\right]\ln(y^2 + 1) - \frac{1}{2}, \tag{3.29}$$

$$l(y) = \frac{X^2(y^2 + 2) - 2X + 1}{(y^2 + 1)} - \frac{2X(X - 1)\ln(y^2 + 1)}{y^2}, \tag{3.30}$$

where Γ_{ab} is defined by eq. (2.46).

Since we are primarily interested in the dynamics of energetic electrons, we also give the high momentum limit of the expressions in eqs. (3.25), (3.26) and (3.27). Intriguingly, they take an appealing form with logarithmically increasing contributions:

$$\{\Delta v_L^1\} \sim -\frac{\Gamma_{ab}}{4\pi}\left(1 + \frac{m_a}{m_b}\right)\frac{1}{u^2}\left(1 + \frac{1}{\ln\Lambda}\left[(X^2 - 1)\ln(y) - \frac{(X - 1)^2}{2}\right]\right), \tag{3.31}$$

$$\{\Delta v_L^2\Delta v_L^2\} \sim \frac{\Gamma_{ab}}{4\pi}\frac{1}{u}\left(1 + \frac{1}{\ln\Lambda}\left[(X^2 - 1)\ln(y) - X(X - 1) - \frac{1}{2}\right]\right), \tag{3.32}$$

$$\{\Delta v_L^1\Delta v_L^1\} \sim \frac{\Gamma_{ab}}{4\pi}\frac{1}{u}\frac{1}{\ln\Lambda}X^2. \tag{3.33}$$

The robustness of this logarithmic form will be investigated in Sections 3.3.3 and 3.3.4 where a different bound electron density, as well as a completely general form factor, are considered.

Finally, the contributions are transformed to an arbitrary frame as in Section 2.2.2

$$\begin{aligned}\{\Delta v^\mu\} &= (\mathbf{e}^\mu \cdot \mathbf{e}_{L,1})\{\Delta v_L^1\} \\ &= -\frac{\Gamma_{ab}}{4\pi}\left(1 + \frac{m_a}{m_b}\right)\frac{u^\mu}{u^3}\left(1 + \frac{g(y)}{\ln\Lambda}\right),\end{aligned} \tag{3.34}$$

$$\begin{aligned}\{\Delta v^\mu\Delta v^\nu\} &= \left[(\mathbf{e}^\mu \cdot \mathbf{e}_{L,2})(\mathbf{e}^\nu \cdot \mathbf{e}_{L,2}) + (\mathbf{e}^\mu \cdot \mathbf{e}_{L,3})(\mathbf{e}^\nu \cdot \mathbf{e}_{L,3})\right]\{\Delta v_L^2\Delta v_L^2\} + \\ &\quad + (\mathbf{e}^\mu \cdot \mathbf{e}_{L,1})(\mathbf{e}^\nu \cdot \mathbf{e}_{L,1})\{\Delta v_L^1\Delta v_L^1\} \\ &= \frac{\Gamma_{ab}}{4\pi}\frac{1}{u}\left[\delta^{\mu\nu} - \frac{u^\mu u^\nu}{u^2}\right]\left(1 + \frac{h(y)}{\ln\Lambda}\right) + \frac{\Gamma_{ab}}{4\pi}\frac{u^\mu u^\nu}{u^3}\frac{l(y)}{\ln\Lambda}.\end{aligned} \tag{3.35}$$

3.2.1 Collision frequencies for cold ions

Our treatment up to now has been general regarding which species collide; the results hold for any species a with charge $\pm e$ colliding with an ion (species b) of arbitrary charge and ionization degree. On the other hand, the main application of an accurate description of screening is to electrons colliding with ions, in which case the mass ratio between the two particles is large. Consequently, it is interesting to investigate a first approximation of the collision operator with a narrow, stationary

ion distribution. Such a distribution is commonly referred to as a "cold" distribution, but note our assumption is $v/v_{Tb} \gg 1$; for example the temperature ratio between the two species may still be of the order unity due to the large mass ratio. This distribution is the special case of the collision operator in Section 2.2.4 with zero thermal velocity of the Maxwellian:

$$f_b(\mathbf{v}) = n_b \delta(\mathbf{v}). \tag{3.36}$$

In this limit the relative velocity and the velocity of the light particle may be taken to be equal, and the collision operator (up to second order, in eqs. (3.1) and (3.2)) takes the form

$$C^{ab} = n_b \left(-\nabla_\mu \left(f_a \{\Delta v^\mu\}_a \right) + \frac{1}{2} \nabla_\mu \nabla_\nu \left(f_a \{\Delta v^\mu \Delta v^\nu\}_a \right) \right). \tag{3.37}$$

For practical reasons (as well as the author's great enthusiasm for relativity) we now bring up the heavy artillery from differential geometry in order to write the collision operator in a general coordinate system, which we specialize to the case of a spherical coordinates. A thorough presentation of differential geometry is outside the scope of this thesis; for the interested reader, see for example Weinberg [30] or Carroll [31].

We use spherical coordinates (v, θ, ϕ) aligned with the velocity vector. The three-dimensional metric (just the spatial coordinates, no time) is

$$g_{\mu\nu} = \begin{pmatrix} 1 & 0 & 0 \\ 0 & v^2 & 0 \\ 0 & 0 & v^2 \sin^2\theta \end{pmatrix}. \tag{3.38}$$

Note that the metric is given in a coordinate basis, where the basis vectors are not normalized. The expressions in eqs. (3.34) and (3.35) in the normalized (vielbein) basis must therefore be transformed. For a diagonal metric the relationship is particularly straightforward. With e_i^μ being the inverse vielbeins and η_{ij} denoting the flat vielbein metric (δ_{ij} for a metric with no time component), the relationship between the vielbein basis and the coordinate basis is

$$g_{\mu\nu} e_i^\mu e_j^\nu = \eta_{ij} \ \Rightarrow \tag{3.39}$$

$$V_{\text{coord}}^\mu = e_i^\mu V_{\text{vielbein}}^i = \text{``} \sqrt{g^{\mu\mu}} V_{\text{vielbein}}^i \text{''}. \tag{3.40}$$

The last expression is clearly not a correct tensor expression but is instructive in an operational sense and is the reason that vielbeins are sometimes referred to as the "square root" of the metric [31]. In the remainder of this section we assume a coordinate basis; and since the collision operator is a scalar the final expressions are coordinate independent.

Throughout this thesis we consistently use covariant notation. For example, the vectors in eq. (3.37) are written with upper indices (e.g. v^μ) since the objects transform as vectors and contravariant tensors. Similarly, we have consistently used ∇_μ to denote gradients, while expressions like ∂_μ are reserved for partial derivatives. In

a Cartesian coordinate system, these are equal but differ in, for example, spherical coordinates. To evaluate the collision operator, we utilize that the divergence can be written nicely, while the second-order differential operator in the Fokker–Planck terms requires Christoffel symbols $\Gamma^{\rho}_{\mu\nu}$:

$$\nabla_{\mu}V^{\mu} = \frac{1}{\sqrt{g}}\partial_{\mu}(\sqrt{g}V^{\mu}) \tag{3.41}$$

$$\nabla_{\nu}T^{\mu\nu} = \partial_{\nu}T^{\mu\nu} + \Gamma^{\mu}_{\nu\rho}T^{\rho\nu} + \Gamma^{\nu}_{\nu\rho}T^{\mu\rho} \tag{3.42}$$

$$\Rightarrow \tag{3.43}$$

$$C^{ab} = \frac{n_b}{\sqrt{g}}\partial_{\mu}\left(\sqrt{g}\Big[f_a\{\Delta v^{\mu}\}_a + \frac{1}{2}\Big(\partial_{\nu}(f_a\{\Delta v^{\mu}\Delta v^{\nu}\}_a) +\right.$$
$$\left. + \Gamma^{\mu}_{\nu\rho}(f_a\{\Delta v^{\rho}\Delta v^{\nu}\}_a) + \Gamma^{\nu}_{\nu\rho}f_a\{\Delta v^{\mu}\Delta v^{\rho}\}_a\Big)\Big]\right), \tag{3.44}$$

where

$$\sqrt{g} = \sqrt{|\det(g_{\mu\nu})|} = v^2\sin\theta, \qquad \Gamma^{\rho}_{\mu\nu} = \frac{1}{2}g^{\rho\sigma}\left(\partial_{\nu}g_{\sigma\mu} + \partial_{\mu}g_{\sigma\nu} - \partial_{\sigma}g_{\mu\nu}\right). \tag{3.45}$$

Carrying out the angular derivatives leaving only the v derivatives, we can write the collision operator as in Section 2.2.4 in the form

$$C^{ab} = \nu_D^{ab}\mathscr{L}(f_a) + \frac{1}{v^2}\frac{\partial}{\partial v}\left(v^3\left[\nu_S^{ab}f_a + \frac{1}{2}\nu_{\parallel}^{ab}v\frac{\partial f_a}{\partial v}\right]\right), \tag{3.46}$$

where the collision frequencies now depend on the functions $g(y)$ and $h(y), l(y)$ defined in eqs. (3.28)-(3.30)

$$\nu_D^{ab} = \frac{n_b}{v^3}\frac{\Gamma_{ab}}{4\pi}\left(1 + \frac{h(y)}{\ln\Lambda}\right) \tag{3.47}$$

$$= \frac{n_b}{v^3}4\pi\left(\frac{m_e}{m_a}r_0c^2Z_0\right)^2\Big(\ln\Lambda$$

$$- X(X-1) + \frac{(X-1)}{2}\left[\frac{X(y^2+2)}{y^2} + 1\right]\ln(y^2+1) - \frac{1}{2}\Big), \tag{3.48}$$

$$\nu_S^{ab} = \frac{n_b}{v^3}\frac{\Gamma_{ab}}{4\pi}\left(\frac{m_a}{m_b}\left[1 + \frac{g(y)}{\ln\Lambda}\right] + \frac{1}{\ln\Lambda}\left[l(y) + \frac{1}{2}yl'(y)\right]\right) \tag{3.49}$$

$$= \frac{n_b}{v^3}4\pi\left(\frac{m_e}{m_a}r_0c^2Z_0\right)^2\left(\left[\frac{(Xy^2+1)^2}{(y^2+1)^2}\right] +\right.$$

$$\left. + \frac{m_a}{m_b}\left[\ln\Lambda + \frac{(X^2-1)\ln(y^2+1)}{2} - \frac{(X-1)^2y^2}{2(y^2+1)}\right]\right), \tag{3.50}$$

$$\nu_{\parallel}^{ab} = \frac{n_b}{v^3}\frac{\Gamma_{ab}}{4\pi}\frac{l(y)}{\ln\Lambda} \tag{3.51}$$

$$= \frac{n_b}{v^3}4\pi\left(\frac{m_e}{m_a}r_0c^2Z_0\right)^2\left(\frac{X^2(y^2+2)-2X+1}{(y^2+1)} - \frac{2X(X-1)\ln(y^2+1)}{y^2}\right). \tag{3.52}$$

As a first check on these results, we neglect the terms of order $1/\ln\Lambda$ and compare to the fully screened frequencies. The collision frequencies agree as required with eqs. (2.85)-(2.87) for collisions with a Maxwellian background, in the limit of zero thermal velocity, $x_b = v/v_{Tb} \gg 1$.

More surprising is that the qualitative behavior of the slowing-down and parallel diffusion frequencies given in eqs. (3.50) and (3.52) is different from their fully screened, leading order $\ln\Lambda$ counterparts. Up to leading order in the Coulomb logarithm, even the Fokker–Planck collision operator with an arbitrary distribution (not necessarily a Maxwellian) contains a factor of m_a/m_b in the first order term corresponding to ν_S^{ab}, see eq. (2.68). For collisions with a cold bulk, the fully screened parallel velocity in eq. (2.87) vanishes identically. With our screening corrections – inherently to next order in $\ln\Lambda$ – the collision frequencies ν_S^{ab} and $\nu_\parallel^{ab}$ are qualitatively different from the fully screened collision frequencies $\nu_{S,\mathrm{fs}}^{ab}$ and $\nu_{\parallel,\mathrm{fs}}^{ab}$ (we use the subscript 'fs' to denote the fully screened version up to leading order in the Coulomb logarithm). Specifically, ν_S^{ab} and $\nu_\parallel^{ab}$ contain terms that do not vanish in the limit of infinite mass ratio m_b/m_a. In contrast, the collision frequency ν_D^{ab} in eq. (3.48) has the same qualitative behavior as $\nu_{D,\mathrm{fs}}^{ab}$: it exhibits an enhancement compared to the completely screened model, especially at high momentum.

The collision frequencies are shown in Figure 3.2. The fully screened form of the deflection frequency, $\nu_{D,\mathrm{fs}}^{ab}$, as given in eq. (2.85), is also included. However we omit the fully screened forms $\nu_{S,\mathrm{fs}}^{ab}$ and $\nu_{\parallel,\mathrm{fs}}^{ab}$ since they practically vanish; as discussed above $\nu_{S,\mathrm{fs}}^{ab}$ is suppressed by a factor $m_a/m_b \sim 10^{-5}$ for a typical electron-ion collision, and $\nu_{\parallel,\mathrm{fs}}^{ab}$ vanish identically. Figure 3.2 shows that even at non-relativistic speeds (normalized momentum $k \lesssim 0.1$), the deflection frequency ν_D^{ab} is enhanced by one order of magnitude compared to the fully screened deflection frequency. This is expected to change the dynamics of a runaway electron beam substantially. At high momentum, the collision frequencies ν_S^{ab} and $\nu_\parallel^{ab}$ are also larger than the fully screened $\nu_{D,\mathrm{fs}}^{ab}$. Further discussion is given after the relativistic generalization is treated in Chapter 4.

We now return to the forms of ν_S^{ab} and $\nu_\parallel^{ab}$ and the large qualitative difference to the fully screened (and leading order in $\ln\Lambda$) corresponding frequencies noted above. Kinematics show that in collisions with heavy particles, the heavy particle remains stationary and there is no energy transfer from the lighter particle to the heavy scatterer. In order to avoid any energy transfer from the light species to the heavy species, the energy loss caused by the frictional collision frequency ν_S^{ab} must cancel the energy gain induced by the diffusive collision frequency $\nu_\parallel^{ab}$. As is shown in Section 3.2.2, the energy transfer scales as m_a/m_b, which means that energy is conserved for the distribution function as a whole. In contrast, ν_S^{ab} and $\nu_\parallel^{ab}$ do not vanish individually in the zero particle to ion mass ratio. This indicates that energy diffusion processes may still affect the population, and consequently individual particles can gain and lose energy in collisions, in such a manner that the energy of the population remains constant. The existence of the slowing-down and parallel diffusion frequencies is therefore a sign that the Fokker–Planck operator exhibits unphysical properties when used to describe screening. Hence the full Boltzmann operator is
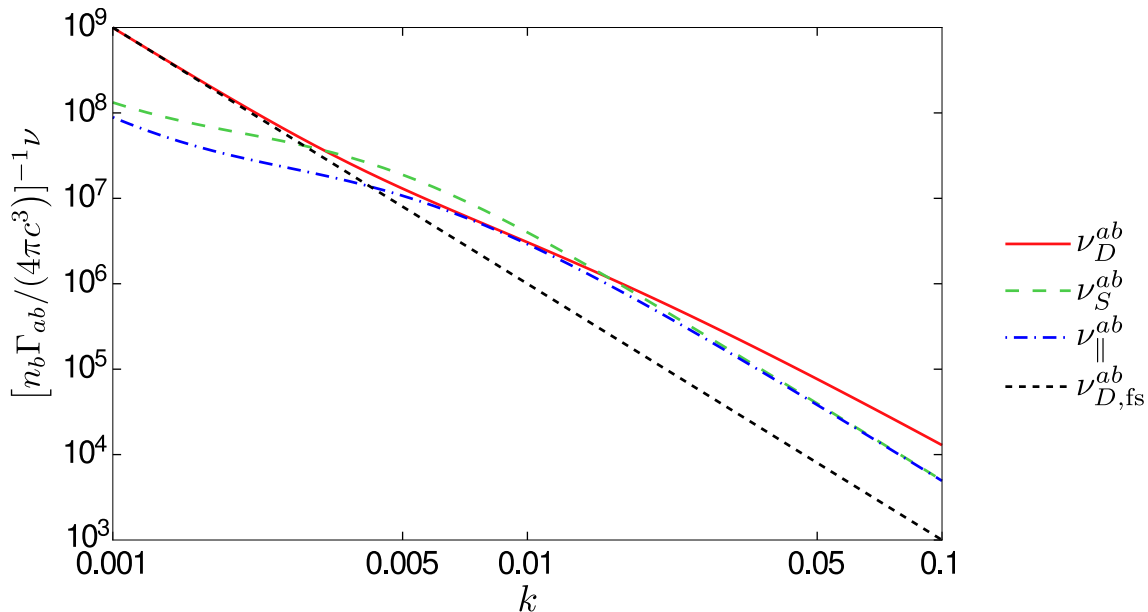
Figure 3.2: The three collision frequencies ν_D (solid red), ν_S (long dashed green) and $\nu_\parallel$ (dash-dotted blue) plotted as a function of normalized momentum $k = p/(m_e c)$ and compared to the fully screened deflection frequency $\nu_{D,\mathrm{fs}}$ in black dashed line. The figure is made with the parameters $X = 10$ and $\ln \Lambda = 20$. We also set $a = a_0$, $m_{ab} = m_a$ to give $y = 2k/\alpha$. The collision frequencies are normalized by setting $n_b \Gamma_{ab}/(4\pi c^3) = 1\,\mathrm{s}^{-1}$. The range of k is limited by the non-relativistic treatment, but already at $k \sim 0.05$ the deflection frequency ν_D is enhanced by one order of magnitude compared to the fully screened formula.

required to obtain the full physical picture and understand the limitations of the Fokker–Planck operator.

In order to get the correct asymptotic limits at low and high momentum (the cross section scaling as Z_0^2 or Z^2 for screening and penetration respectively), the functions $g(y)$ and $h(y)$ as defined in eqs. (3.25) and (3.26) are needed, providing the interpolation between the fully screened and the bare nucleus interactions. In contrast, $l(y)$, from the velocity moment $\{\Delta u_L^1 \Delta u_L^1\}$ in eq. (3.27), is unnecessary to achieve these two limits; see more in Section 3.3.1. It is precisely $l(y)$ that causes the unphysical energy diffusion; without it both ν_S^{ab} and $\nu_\parallel^{ab}$ as given in eqs. (3.49) and (3.51) vanish identically. The three collision frequencies would have the same qualitative form in regards to energy conservation as the fully screened frequencies in eqs. (2.85)-(2.87).

3.2.2 Energy loss in the cold ion limit

Computing the energy loss in the cold ion limit is of physical interest to see if the screening effects considerably enhance the energy loss experienced by incident electrons. Furthermore it is useful for validation: the energy loss must vanish in the limit of infinite ratio m_b/m_a. Thus, this section both provides a qualitative check and a quantitative result.

The total energy loss rate from a distribution of particles is given by the energy moment of the collision operator

$$Q^{ab} = \int d\mathbf{v} \frac{mv^2}{2} C^{ab}.$$ (3.53)

With the collision operator in the form of eq. (3.46), we first take the Lorentz operator part:

$$
\begin{aligned}
Q_{\nu_D}^{ab} &= \int v^2 dv \sin\theta d\theta d\phi \frac{mv^2}{2} \nu_D^{ab} \mathscr{L}(f_a) \\
&= \frac{m}{2} \int v^4 dv d\theta d\phi \nu_D^{ab} \frac{1}{2} \left[\frac{\partial}{\partial\theta}\left(\sin\theta \frac{\partial f_a}{\partial\theta}\right) + \frac{1}{\sin\theta}\frac{\partial^2 f_a}{\partial\phi^2} \right] \\
&\propto \int v^4 dv d\phi \left[\sin\theta \frac{\partial f_a}{\partial\theta} \right]_0^\pi + \int v^4 dv d\theta \frac{1}{\sin\theta}\left[\frac{\partial f_a}{\partial\phi} \right]_0^{2\pi} \\
&= 0,
\end{aligned}
$$ (3.54)

provided $\partial f_a / \partial\theta$ is bounded in v and using the periodicity of f_a in ϕ.

The energy loss is thus

$$Q^{ab} = \frac{m}{2} \int v^4 dv d\Omega \frac{1}{v^2} \frac{\partial}{\partial v}\left[v^3 \left(\nu_S^{ab} f_a + \frac{1}{2}\nu_\parallel^{ab} v \frac{\partial f_a}{\partial v} \right) \right].$$ (3.55)

Integrating by parts and assuming that the distribution function itself vanishes fast enough as the velocity approaches infinity, we find

$$
\begin{aligned}
Q^{ab} &= -m \int dv d\Omega \, v \left[v^3 \left(\nu_S^{ab} f_a + \frac{1}{2}\nu_\parallel^{ab} v \frac{\partial f_a}{\partial v} \right) \right] \\
&= -\int d\mathbf{v} \frac{mv^2}{2} 2 \left[\nu_S^{ab} - \frac{1}{v^4}\frac{\partial}{\partial v}\left(\frac{v^5}{2}\nu_\parallel^{ab} \right) \right] f_a \\
&\equiv -\int d\mathbf{v} \frac{mv^2}{2} \nu_E^{ab} f_a,
\end{aligned}
$$ (3.56)

where we performed another integration by parts of the second term and in the last step introduced ν_E^{ab} as the energy loss frequency. Substituting the collision frequencies from eqs. (3.49) and (3.51) yields

$$
\begin{aligned}
\nu_E^{ab} &= 2\frac{n_b}{v^3}\frac{\Gamma_{ab}}{4\pi}\left[\frac{m_a}{m_b}\left(1 + \frac{g(y)}{\ln\Lambda}\right) + \frac{1}{\ln\Lambda}\left(l(y) + \frac{1}{2}yl'(y)\right) \right. \\
&\qquad \left. - \frac{1}{\ln\Lambda}\left(l(y) + \frac{1}{2}yl'(y)\right) \right] \\
&= 2\frac{n_b}{v^3}\frac{\Gamma_{ab}}{4\pi}\frac{m_a}{m_b}\left(1 + \frac{g(y)}{\ln\Lambda}\right) \\
&= 2\frac{n_b}{v^3}\frac{\Gamma_{ab}}{4\pi}\frac{m_a}{m_b}\left(1 + \frac{1}{\ln\Lambda}\left[\frac{(X^2-1)\ln(y^2+1)}{2} - \frac{(X-1)^2 y^2}{2(y^2+1)} \right]\right).
\end{aligned}
$$ (3.57)

In the limit $m_a/m_b \to 0$, the energy loss vanishes as expected for collisions with infinitely heavy particles. Despite the large enhancement of the slowing-down frequency, the energy losses from the friction force are entirely cancelled by the parallel velocity diffusion frequency. It is interesting that the contribution from the velocity moment $\{\Delta u_L^1 \Delta u_L^1\}$ vanishes in the energy loss moment of the collision operator. A detailed calculation shows that (apart from the zeroth moment which gives number density conservation as required from eq. (2.69)) it is only in the energy moment that the contribution from $\{\Delta u_L^1 \Delta u_L^1\}$ vanishes.

The energy loss frequency is still negligible compared to the electron-electron energy loss collision frequency. The collision frequency for electron-electron collisions assuming a cold bulk is readily obtained in the fully screened limits of our expressions but is also given in the literature, see for example Hinton [25]

$$\nu_E^{ee} = 2\frac{n_e}{v^3}4\pi \left(r_0 c^2\right)^2 \ln \Lambda, \tag{3.58}$$

$$\nu_E^{ei} = 2\frac{n_i}{v^3}4\pi \left(r_0 c^2 Z_0\right)^2 \frac{m_e}{m_i}\left(\ln \Lambda + g(y)\right). \tag{3.59}$$

As a rough estimate, we take a doubly ionized argon atom which corresponds to the following parameters and a temperature of $28\,\mathrm{eV}$ [32] :

$$\frac{m_e}{m_i} \approx \frac{1}{2Z \cdot 1823} \approx 10^{-5}, \quad X = 10, \quad \frac{n_e}{n_i} = 2, \quad Z_0 = 2, \quad \ln \Lambda = 20. \tag{3.60}$$

This factor is so small that the enhancement in the collision operator does not help; for moderately charged ions the energy loss is negligible compared to that from electron-electron collisions. Even for a singly ionized uranium plasma, the electron-ion energy loss frequency will only be around $10\,\%$ of the electron-electron energy loss frequency. Accordingly, an accurate treatment of screening mainly affects the distribution function by collisions that conserve the total energy of the species: deflection caused by ν_D^{ab} and diffusion by ν_S^{ab} and $\nu_\parallel^{ab}$ as discussed in the previous section.

3.3 Robustness of the results

In this section we critically review our model and the results. Firstly, as a check on our results, the low and high momentum behaviors are investigated. We also look briefly at the validity of the Fokker–Planck treatment. Since our screening corrections are independent of the Coulomb logarithm (and therefore of next to leading order in the Coulomb logarithm), large corrections will challenge the dominance of the small-angle collision terms. The higher order terms in the Taylor expanded Boltzmann operator are therefore compared to the second order Fokker–Planck terms. Finally, we study the sensitivity to the choice of a specific model for the form factor, and find a general argument that the high-momentum behavior should be the same regardless of the model.

3.3.1 Asymptotic limits

A validation of our model is that the expected asymptotic behavior is reproduced. As the form factor approaches N_e and 0 in the low and high momentum limits, the "screened nuclear charge" should approach $Z - N_e = Z_0$ and Z respectively, up to leading order in $\ln \Lambda$, as discussed in Section 2.3.2. For the three moments in eqs. (3.25), (3.26) and (3.27), this corresponds to the corrections $g(y)$, $h(y)$ and $l(y)$ being negligible for low momenta, and for high momenta we require an enhancement by a factor of X^2 compared to full screening, corresponding to complete penetration of the ion. We wish to verify the following limits

$$\{\Delta v_L^1\} = -\frac{\Gamma_{ab}}{4\pi}\left(1 + \frac{m_a}{m_b}\right)\frac{1}{u^2}\left(1 + \frac{g(y)}{\ln\Lambda}\right) \tag{3.61}$$

$$\xrightarrow[p\to\infty]{?} -\frac{\Gamma_{ab}}{4\pi}\left(1 + \frac{m_a}{m_b}\right)\frac{1}{u^2}X^2 + \mathcal{O}\left(\frac{1}{\ln\Lambda}\right),$$

$$\{\Delta v_L^2 \Delta v_L^2\} = \frac{\Gamma_{ab}}{4\pi}\frac{1}{u}\left(1 + \frac{h(y)}{\ln\Lambda}\right) \xrightarrow[p\to\infty]{?} \frac{\Gamma_{ab}}{4\pi}\frac{1}{u}X^2 + \mathcal{O}\left(\frac{1}{\ln\Lambda}\right), \tag{3.62}$$

$$\{\Delta v_L^1 \Delta v_L^1\} = \frac{\Gamma_{ab}}{4\pi}\frac{1}{u}\frac{l(y)}{\ln\Lambda} \xrightarrow[p\to\infty]{?} \mathcal{O}\left(\frac{1}{\ln\Lambda}\right). \tag{3.63}$$

The low momentum limit is clearly fulfilled; the corrections $g(y)$, $h(y)$ and $l(y)$ given in eqs. (3.28)-(3.30) are all small compared to $\ln\Lambda$. The high momentum limit is not as straightforward as both $g(y)$ and $h(y)$ diverge logarithmically. However, only at extremely high momentum (quantified below) is this high momentum limit of complete ion penetration reached. At such high momentum the neglected terms of order Λ^{-1} mentioned in Section 3.2 start to play a role; indeed this can be seen to solve the problem and give the correct limits. When these terms are restored, we get for eq. (3.61)

$$1 + \frac{g(y)}{\ln\Lambda} = 1 + \frac{1}{\ln\Lambda}\frac{1}{2}(X^2 - 1)\ln\left(\frac{1 + y^2}{1 + y^2\Lambda^{-2}}\right)$$

$$- \frac{1}{\ln\Lambda}(X - 1)^2\frac{y^2}{2(1 + y^2)}\frac{(1 - \Lambda^{-2})}{(1 + y^2\Lambda^{-2})}$$

$$\to \begin{cases} 0, & y \to 0, \\ X^2, & y \to \infty. \end{cases} \tag{3.64}$$

We thus get the expected limit, but since $\Lambda \gg 1$ this limit will be obtained extremely slowly. The transition occurs where the momentum parameter y defined in eq. (3.6) has values around $y \sim \Lambda \sim \exp(20) \sim 5{\cdot}10^8$. As can be seen in Figure 3.3 with $\ln\Lambda = 20$ and $X = 10$, the expected limit with an enhancement of $X^2 = 100$ is achieved by the full velocity moments at very high velocities, while the simplified expressions continue to grow logarithmically beyond the theoretical limit. The approximate transition is confirmed with a transition around $y \sim 10^9$. In terms of the normalized momentum $k = p/(m_e c)$ it corresponds to $k \sim 4 \cdot 10^6$, or a kinetic energy of $2\,\mathrm{TeV}$, and thus is far beyond relevant momenta, even if a relativistic collision operator were considered. We note that the expected limit is obtained in the full version, but we can safely use the approximated results.

The same analysis of the asymptotic limits holds for $\{\Delta v_L^2 \Delta v_L^2\}$ and $\{\Delta v_L^1 \Delta v_L^1\}$. What is interesting to note is that $\{\Delta v_L^1 \Delta v_L^1\}$ will approach the high momentum limit much faster than the other two terms, see Figure 3.3. This has the effect that while $\{\Delta v_L^1 \Delta v_L^1\}$ is small in most of momentum space, it is relatively more important in a small region around $y \sim 1$. In this region, $\{\Delta v_L^1\}$ and $\{\Delta v_L^2 \Delta v_L^2\}$ have not yet grown far above the low momentum (or full screening) limit, while $\{\Delta v_L^1 \Delta v_L^1\}$ has almost reached its high momentum limit, corresponding to no screening. Since $\{\Delta v_L^1 \Delta v_L^1\}$ comes without the prefactor of $\ln \Lambda$, which is related to small angle dominance, it is therefore possible that higher order corrections and thus large-angle scattering will be of importance in this region. This issue will be the topic of the following section.
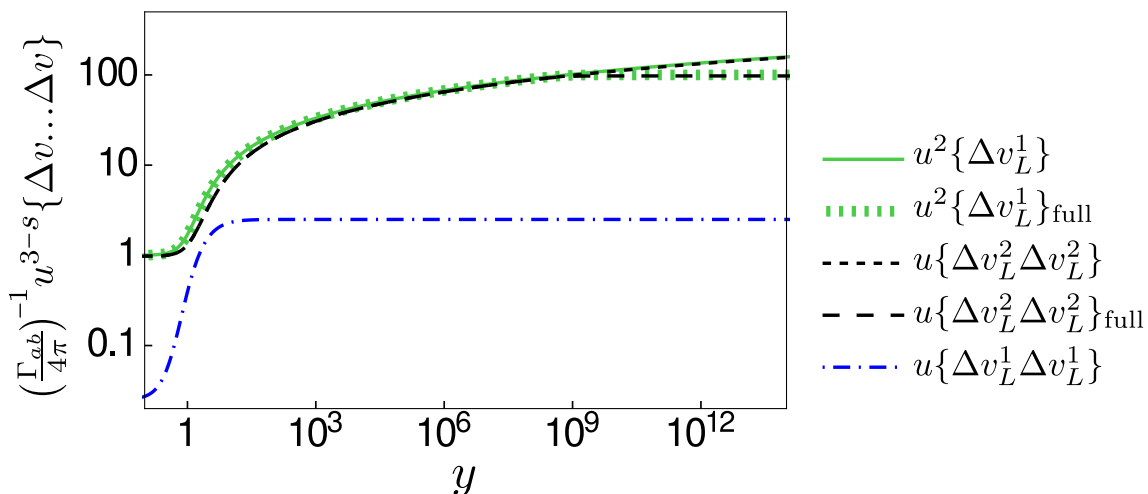
Figure 3.3: The figure shows the three velocity moments $\{\Delta v_L^1\}$ (solid green line), $\{\Delta v_L^2 \Delta v_L^2\}$ (dashed black line) and $\{\Delta v_L^1 \Delta v_L^1\}$ (dash-dotted blue), all with the velocity dependence in eqs. (3.25), (3.26) and (3.27) multiplied out for the clarity of plotting. These quantities were compared to the their full counterparts, where terms of order Λ^{-1} were not neglected. $\{\Delta v_L^1\}_{\text{full}}$ can be seen in dotted green line, while $\{\Delta v_L^2 \Delta v_L^2\}_{\text{full}}$ is denoted by a long dashed black line. The dependence is shown as a function of the dimensionless momentum parameter $y \sim 300k$, as defined in eq. (3.6) and where $k = p/(m_e c)$. The parameters $X = 10$ and $\ln \Lambda = 20$ were used, together with $a = a_0$, $m_{ab} = m_a$ and a normalization according to $\Gamma_{ab}/(4\pi) = 1$.

3.3.2 Higher order terms

This section aims to introduce an estimate of the magnitude of terms of different orders in the small deflection angle[1] expansion of the Boltzmann operator. If the terms are small, it can be expected that there will only be a small difference between the Boltzmann operator and the Fokker–Planck operator (which equals the two first terms of the Boltzmann operator, see Section 2.1.2) and the use of the Fokker–Planck operator is justified.

---

[1] Technically, the expansion is done for small momentum transfer in each collision, which is closely related to a small deflection angle.

In order to get a rough estimate of the relative magnitude of the higher order terms, consider eqs. (3.1) and (3.13). For a fixed relative velocity, the quantity of interest will be of order

$$\left(\frac{\partial f_a}{\partial t}\right)_c\bigg|_{\text{terms of order } s} \sim \frac{2^s}{s!} A_{mn} I_{lmn}(y). \tag{3.65}$$

An upper estimate for I_{lmn} can be found by letting the form factor vanish in the limit of large velocities:

$$I_{lmn}(u) \leq Z^2 \int_0^1 dx \frac{(1-x^2)^{m+n}}{x^{3-s-l}} = Z^2 \frac{(m+n)!(l+m+n-2)!}{2(s-1)!} \leq \frac{Z^2}{2(s-1)}, \tag{3.66}$$

where the maximum value is obtained for $l = s$. The lower integral limit can be taken to zero for all terms $s + l \geq 3$, since these higher order terms do not diverge in this limit, as opposed to the leading order terms in the Coulomb logarithm. The contribution from the angular integral defined in eq. (3.7) obeys $A_{mn} \leq 2\pi$ and is also maximized for $l = s$, therefore

$$\left(\frac{\partial f_a}{\partial t}\right)_c\bigg|_{\text{terms of order } s} \sim \pi Z^2 \frac{2^s}{s!(s-1)} \to 0, \text{ as } s \to \infty. \tag{3.67}$$

It thus seems as if the Boltzmann operator may converge in its Taylor expanded form and the first terms will be most important. However, this expression neglects the effects of the differentiation of different powers of v, as well as the number of terms of each order. Another complication is that the higher order terms can reach their high momentum limits faster than the leading $\ln \Lambda$ terms. This is demonstrated in Figure 3.4 where there is a region of intermediate momentum where higher order terms are relatively large compared to the lower order terms. This transition region is approximately where the dimensionless momentum $y \sim 1$, which coincides with the transition region from full screening to no screening of the cross section as shown in Section 3.2. This behavior agrees with the reasoning in Section 3.2; around the transition between the low and high momentum behavior, the cross section falls more slowly than the power of $\sin^4(\theta/2)$ otherwise observed, and small-angle collisions need not dominate.

For future work it would therefore be valuable to investigate the effect of screened nuclei with the full Boltzmann integral operator, which accounts for large angle collisions. Using the Boltzmann operator is particularly motivated for heavy ions with low degree of ionization. The extent to which the higher order terms are suppressed is closely connected to the relation between the two large parameters that are present in this problem: the ratio $X^2/\ln \Lambda$. When the Coulomb logarithm is less dominant, it is a sign that large angle collisions may contribute. In cases (b) and (c) in Figure 3.4, this ratio is large and consequently some higher order terms may be significant.

3.3.3 General features

An accurate modeling of screened nuclei may be expected to have the greatest impact at high momentum, which makes it the most important region of phase space to
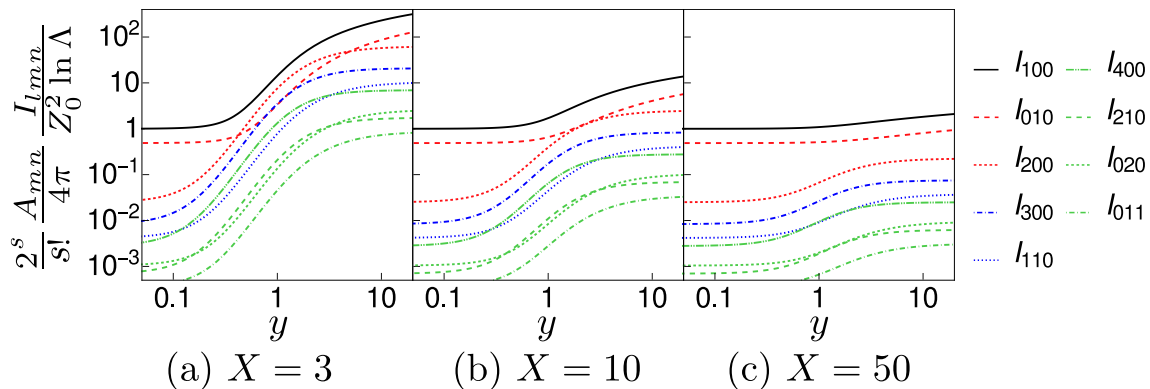
Figure 3.4: Comparison between terms in eq. (3.13) of different order in the Taylor expanded Fokker–Planck operator. The terms $\frac{2^s}{s!}\frac{A_{mn}}{4\pi}\frac{I_{lmn}}{Z_0^2 \ln \Lambda}$ are plotted for $\ln \Lambda = 20$ as a function of the dimensionless momentum parameter y defined in eq. (3.6). The color coding for the terms of successive order is shown in the key in the figure. The three subfigures show the results for different values of the inverse ionization degree X. The two terms I_{100} and I_{010} containing $\ln \Lambda$ dominate for low and high momentum, whereas, especially for large X, the higher order terms can be significant around $y \sim 1$.

examine. The results given here using a non-relativistic operator will obviously not be applicable all the way to the interesting momentum region of runaway particles, but their effect, for example on the runaway growth rate, may still be investigated. Additionally, the results presented here will serve as a test case to compare with the relativistic version in Chapter 4.

As noted in Section 3.2, the velocity moments in eqs. (3.25), (3.26) and (3.27) take an appealing, logarithmic form in the high momentum limit:

$$\{\Delta v_L^1\} \sim -\frac{\Gamma_{ab}}{4\pi}\left(1 + \frac{m_a}{m_b}\right)\frac{1}{u^2}\left(1 + \frac{1}{\ln \Lambda}\left[(X^2 - 1)\ln(y) - \frac{(X-1)^2}{2}\right]\right), \quad (3.68)$$

$$\{\Delta v_L^2 \Delta v_L^2\} \sim \frac{\Gamma_{ab}}{4\pi}\frac{1}{u}\left(1 + \frac{1}{\ln \Lambda}\left[(X^2 - 1)\ln(y) - X(X-1) - \frac{1}{2}\right]\right), \quad (3.69)$$

$$\{\Delta v_L^1 \Delta v_L^1\} \sim \frac{\Gamma_{ab}}{4\pi}\frac{1}{u}\frac{1}{\ln \Lambda}X^2. \quad (3.70)$$

To further test the sensitivity of the collision operator to the assumed electron density of the ion, we now undertake a similar analysis as that given in Section 3.2, with a model which is very different to the Yukawa model. The model we take is a spherical shell of infinitesimal width, here denoted as a δ-shell model, located at $r = a$ with the same mean distance to the nucleus as the average Yukawa model density. This model is practical and highly simplified; however it does offer a length scale and normalization factor. The bound electron density and corresponding form factor are thus:

$$n_e(r) = N_e \frac{\lambda^2}{4\pi}\delta(r - a); \quad F(q) = N_e \frac{\sin(qa)}{qa} = N_e \frac{\sin(yx)}{yx}. \quad (3.71)$$

The cross sections in eq. (2.91) using the Yukawa and the shell models are shown together with the limiting behaviors at low and high momentum in Figure 3.5. The result shows the shell model causes a small oscillation and the transition between the limiting behaviors is at slightly higher momentum than for the Yukawa model.
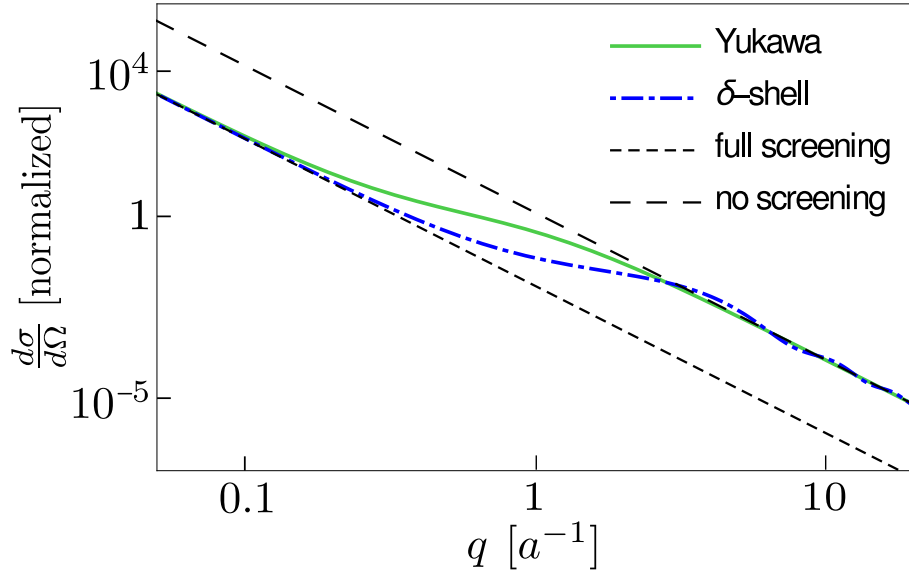
Figure 3.5: The shape of the cross section highlighted for the Yukawa model (solid green) along with the cross section for a δ-shell (dash-dotted blue). The figure shows the cross section on a log-log scale as a function of $q = \sin(\theta/2)y/a$, where $y \sim 2k/\alpha$ is the dimensionless momentum parameter, $k = p/(m_e c)$ is the normalized momentum, a is a length scale of the ion and θ is the deflection angle. The two models exhibit slightly different transitions from full screening (dashed black line) to the higher cross section with no screening (long dashed black line): the Yukawa model has a transition at lower momentum corresponding to a larger effective scale a.

Analytical formulas for the velocity moments corresponding to the Yukawa model moments in eqs. (3.25), (3.26) and (3.27), are available in terms of the Cosine integral

$$\mathrm{Ci}(x) = -\int_x^\infty \frac{\cos t}{t} dt = \gamma_E + \ln(x) - \mathrm{Cin}(x), \qquad (3.72)$$

where $\mathrm{Ci}(x) \xrightarrow[x\to\infty]{} 0$, and $\mathrm{Cin}(x) \xrightarrow[x\to 0]{} 0$. $\gamma_E \approx 0.58$ is the Euler–Mascheroni constant. From the definitions of the contributions to the collision operator eqs. (3.25), (3.26) and (3.27), we look at the corrections to the FP terms and then compare them to eqs. (3.28)-(3.30) for $g(y)$, $h(y)$ and $l(y)$ derived for the Yukawa model.

$$g_\delta(y) = -2X(X-1)\left[\mathrm{Ci}(y) + 1 - \frac{\sin y}{y}\right] + \left(X^2 - 1\right)[\ln(y) + \gamma_E] +$$

$$\frac{1}{2}(X-1)^2\left[2\mathrm{Ci}(2y) - \frac{\sin^2(y)}{y^2} - \frac{\sin(2y)}{y} + 3 - 2\ln(2)\right], \qquad (3.73)$$

$$l_\delta(y) = X^2 - \frac{4X(X-1)(1-\cos(y))}{y^2}$$
$$+ \frac{(X-1)^2(-\text{Ci}(2y) + \ln(2y) + \gamma_E)}{y^2}, \tag{3.74}$$

$$h_\delta(y) = g_\delta(y) - l_\delta(y)/2. \tag{3.75}$$

Once again, we see the same dominating logarithmic dependence in momentum. Rescaling the momentum parameter, we see that the results of the Yukawa model and the shell model are similar, as is shown in Figure 3.6. Demanding $g_\delta(y(a_\delta)) = g_Y(y(a_Y))$, a detailed calculation shows that the relation between the length scales to match the high-momentum limit is

$$\frac{a_\delta}{a_Y} = \exp\left(-\gamma_E + \frac{2 + (X-1)\ln 2}{X+1}\right). \tag{3.76}$$

For large inverse ionization degree X, this corresponds to $a_\delta/a_Y \approx 1.12$, while $X = 10$ gives $a_Y/a_\delta \approx 1.19$.

(a) $a_\delta = a_Y$ (b) $a_\delta = 1.19 a_Y$
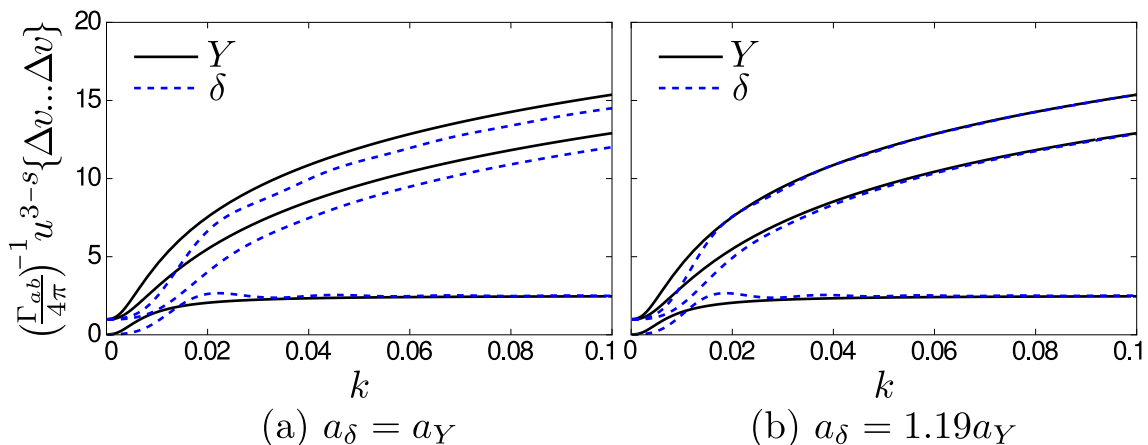
Figure 3.6: $X = 10$, $\ln \Lambda = 20$. Comparing the Yukawa model and the shell model by examining the three velocity moments in the Fokker–Planck operator: $\{\Delta v_L^1\}$, $\{\Delta v_L^2 \Delta v_L^2\}$ and $\{\Delta v_L^1 \Delta v_L^1\}$. The velocity dependence in eqs. (3.25), (3.26) and (3.27) is multiplied out for the clarity of plotting. The solid black lines are Yukawa terms while the dashed blue lines are the corresponding terms with a δ-shell. Both are plotted as a function of normalized momentum k, and with the parameters $X = 10$, $\ln \Lambda = 20$, $a = a_0$, $m_{ab} = m_a$ and the prefactor $\Gamma_{ab}/(4\pi)$ set to unity. (a) shows the difference between the two models without any scaling; $a_Y = a_\delta$. There is then a small discrepancy between the models. The two models however can be made to overlap almost exactly if the atomic length scales are shifted, which is seen in (b).

In conclusion, our results indicate that the physical picture of the high energy screening effect is robust in regard to which nuclear model is used. This promising result is considered and further developed in the next Section 3.3.4.

3.3.4 Motivating high momentum behavior

In the two widely different bound electron density models considered in this chapter, we find that the leading order behavior at high momentum is

$$\{\Delta v_L^1\} \sim -\frac{\Gamma_{ab}}{4\pi}\left(1 + \frac{m_a}{m_b}\right)\frac{1}{u^2}\left(1 + \frac{1}{\ln\Lambda}\ln y + \text{const}\right). \tag{3.77}$$

Except for the velocity scaling (different powers of u), $\{\Delta v_L^1\}$ and $\{\Delta v_L^2 \Delta v_L^2\}$ are similar, while as before $\{\Delta v_L^1 \Delta v_L^1\}$ is small, see eqs. (3.31)-(3.33). A modest attempt to explain this, and argue for its generality, is provided in this section. If the logarithmic behavior is proved to be general, constant terms can be taken care of by rescaling the atomic length scale a as was done in Section 3.3.3, and we can thus effectively – with an arbitrary model for the form factor – reproduce the "true" physical behavior at high momentum. This is particularly interesting if the same logarithmic growth would hold up to relativistic speeds, as it would ease the modeling of the effect on runaway electron dynamics. The motivation below is made for non-relativistic cross sections, but the same argument holds for the relativistic case.

Assume

$$y \gg 1, \quad y\theta_{\min} \ll 1, \tag{3.78}$$

which roughly corresponds to an interval of the normalized momentum $10^{-2} \ll k = p/(m_e c) \ll 10^6$. We also know that we have a fundamental length scale a, with $t = yx = qa$, and that $F(t \ll 1) \approx N_e, F(t \gg 1) \approx 0$. We then have for the integral I_{100}, defined in eq. (3.14) and related to the moment $\{\Delta v_L^1\}$ by eq. (3.24),

$$I_{100} = \int_{\theta_{\min}/2}^1 \frac{(Z - F(yx))^2}{x}dx$$
$$= Z^2\ln\Lambda + \int_{y\theta_{\min}/2}^y \frac{-2ZF(t) + F(t)^2}{t}dt. \tag{3.79}$$

Splitting the integral into two pieces:

$$\int_{y\theta_{\min}/2}^y \frac{F(t)}{t}dt = \int_{y\theta_{\min}/2}^1 \frac{F(t)}{t}dt + \int_1^y \frac{F(t)}{t}dt$$
$$= \left[\ln t F(t)\right]_{y\theta_{\min}/2}^1 - \int_{y\theta_{\min}/2}^1 \ln t \, F'(t)dt + \int_1^y \frac{F(t)}{t}dt. \tag{3.80}$$

We will now show that the first term gives the logarithmic behavior, while the second two contribute with at most a constant. For the first term in eq. (3.80)

$$\left[\ln t F(t)\right]_{y\theta_{\min}/2}^1 = -\ln\left(y\frac{\theta_{\min}}{2}\right)F\left(y\frac{\theta_{\min}}{2}\right)$$
$$\approx (\ln\Lambda - \ln y)N_e. \tag{3.81}$$

As for the second term in eq. (3.80), the first derivative of the form factor vanishes identically for small arguments. This is because the atom has a spherically symmetric

potential, which makes the mean dipole moment ($\propto \int d^3r\, \mathbf{r} n(\mathbf{r})$) vanish [22]. We may therefore expect that the exact limit $y\theta_{\min}/2$ is unimportant as long as it is sufficiently small, and consequently

$$\int_{y\theta_{\min}/2}^{1} \ln t\, F'(t)\, dt \approx \text{const.} \tag{3.82}$$

As for the third term in eq. (3.80), we utilize that $F(y) \ll 1$ and the upper limit should not matter; we can extend it to infinity.

$$\int_{1}^{y} \frac{F(t)}{t} dt \approx \int_{1}^{\infty} \frac{F(t)}{t} dt = \text{const.} \tag{3.83}$$

Equation (3.80) therefore reads

$$\int_{y\theta_{\min}/2}^{y} dt \frac{F(t)}{t} = (\ln\Lambda - \ln y)N_e + \text{const.} \tag{3.84}$$

The corresponding calculation for $F(t)^2$ yields the same with N_e replaced with N_e^2, which inserted into eq. (3.79) gives

$$\begin{aligned} I_{100} &= Z^2 \ln\Lambda - 2N_e Z(\ln\Lambda - \ln y) + N_e^2(\ln\Lambda - \ln y) + \text{const} \\ &= Z_0^2\Big(\ln\Lambda + (X^2 - 1)\ln y + C\Big), \quad \text{for } 1 \ll y \ll 1/(\theta_{\min}/2). \end{aligned} \tag{3.85}$$

This gives exactly eq. (3.77). This result indicates that since this constant could be absorbed into a rescaling of y which would correspond to rescaling the length scale a, the final result at high momenta is insensitive to the chosen model for the bound electron density, as long as it satisfies the asymptotic values and has a defined length scale. Of course this scaling constant must be determined, but the problem is reduced dramatically from finding a function to a one-parameter problem.

4

Relativistic Screened Collision Operator

Since the difference between the description of collisions with fully screened ions and an accurate treatment of screening is greatest at high momentum, a relativistic formulation of the problem is necessary. Additionally, a relativistic formulation is needed to describe runaway particles. A complication in deriving the relativistic collision operator compared to the non-relativistic case is the more involved kinematics when describing the collision process in the center of mass frame. Accordingly, the more general case of arbitrary mass ratios is only considered in the non-relativistic derivation, while the relativistic treatment given here considers only the limit of small incoming particle to ion mass ratio, which is accurate for collisions between electrons (or positrons) and ions.[1] In the small particle-to-ion mass limit, the relativistic collision operator is straightforward to derive using the method of Chapter 3. In this chapter we derive the corresponding relativistic expressions and investigate their behavior using the Yukawa model for the electron cloud of the ion. As the discussions about higher order terms and limiting behaviors are similar to the non-relativistic collision operator, we mainly focus on the robustness of the model and a comparison with the non-relativistic results.

4.1 Collision operator terms

To be consistent with the limit of infinite ion to particle mass ratio, $m_a/m_b \ll 1$, we specialize to the mass $m_a = m_e$ of the colliding particle. For heavy ions, we use the distribution of a cold bulk, as in Section 3.2.1:

$$f_b(\mathbf{p}') = n_b \delta(\mathbf{p}'), \tag{4.1}$$

where we use relativistic momentum, $\mathbf{p} = \gamma m \mathbf{v}$. In this limit the relative velocity in eqs. (2.22) and (2.23) is simplified. Since $E_e^2/c^2 = |\mathbf{p}|^2 + m_e^2 c^2$, $E_i^2 = c^2 m_i^2$ we get

$$\frac{c}{(p^0)'p^0} \sqrt{(p^j p_j')^2 - m_e^2 m_i^2 c^4} = \frac{c}{p^0 m_i c} \sqrt{(m_e^2 c^2 + |\mathbf{p}|^2) m_i^2 c^2 - m_e^2 m_i^2 c^4}$$

$$= \frac{|\mathbf{p}|}{\gamma m_e}. \tag{4.2}$$

---

[1] Relativistic effects will enhance the mass ratio by the Lorentz factor γ, but the assumption still holds for realistic runaway electron scenarios.

The relativistic Fokker–Planck collision operator in eq. (2.21) then takes the simplified form

$$C^{ei} = -\nabla_k \left(f_e \{\Delta p^k\}_e \right) + \frac{1}{2} \nabla_k \nabla_j \left(f_e \{\Delta p^k \Delta p^j\}_e \right), \tag{4.3}$$

where the non-relativistic velocity moments from Chapter 3 are replaced by the relativistic momentum moments

$$\{\Delta p^l \Delta p^j \dots \Delta p^k\} = \int d\Omega \frac{d\sigma}{d\Omega} \frac{|\mathbf{p}|}{\gamma m_e} \Delta p^l \Delta p^j \dots \Delta p^k. \tag{4.4}$$

In the cold bulk limit considered here, the kinematics is the same as in the non-relativistic case. By energy conservation there is no change in the zeroth component of the velocity four-vector, giving in the local center of mass frame

$$\begin{aligned}
\Delta p_L^0 &= 0, \\
\Delta p_L^1 &= -2p \sin^2(\theta/2), \\
\Delta p_L^2 &= 2p \cos(\theta/2) \sin(\theta/2) \cos\phi, \\
\Delta p_L^3 &= 2p \cos(\theta/2) \sin(\theta/2) \sin\phi,
\end{aligned} \tag{4.5}$$

where $p = |\mathbf{p}|$. With no change in the zeroth component, only the three spatial derivatives will matter and we can replace the Latin indices denoting the four space-time variables with the Greek indices for spatial variables.

In the Born approximation, the cross section needed for eq. (4.4) is given by eq. (2.94),

$$d\Omega \frac{d\sigma}{d\Omega} = \frac{r_0^2 [Z - F(q)]^2}{2} \frac{\cos(\theta/2)}{\sin^3(\theta/2)} \frac{1}{k^4} \left(\cos^2(\theta/2)k^2 + 1 \right) d\theta d\phi, \tag{4.6}$$

where $q = 2\sin(\theta/2)p/\hbar$.

Similarly to the treatment in eq. (3.13), we can find the general form of the terms contributing to the collision operator as the following

$$\{(\Delta p_L^1)^l (\Delta p_L^2)^{2m} (\Delta p_L^3)^{2n}\} = (-1)^l 2^s A_{mn} \left(r_0 c^2\right)^2 \frac{m_e^s}{\gamma (ck)^{3-s}} I_{lmn,\mathrm{rel}}(p), \tag{4.7}$$

where

$$I_{lmn,\mathrm{rel}}(p) = \int_{\theta_{\min}/2}^1 dx \frac{(1-x^2)^{m+n}}{x^{3-s-l}} \left((1-x^2)\frac{p^2}{(m_e c)^2} + 1 \right) \left[Z - F\left(\frac{y}{a}\right) \right]^2, \tag{4.8}$$

and we recall $s = l + 2m + 2n$. We once again parametrize with the normalized momentum $k = p/(m_e c)$ and y in eq. (3.6),

$$y = \frac{a}{a_0} \frac{2k}{\alpha}. \tag{4.9}$$

In the nonrelativistic limit, $I_{lmn,\mathrm{rel}} \to I_{lmn}$, and $\gamma(ck)^3 \to u^3$. In order to reconnect to the non-relativistic case, note that the factor of $1/m_e^s$ will cancel when converting from derivatives with respect to momentum p to velocity derivatives u in eq. (4.3), and the non-relativistic case in eq. (3.13) is reproduced.

4.2 Results with the Yukawa model

In this section, we obtain the relativistic expressions corresponding to the Yukawa potential model in Section 3.2. The expression for the integral in eq. (4.8) is then

$$I_{lmn,\text{rel}}(p) = \int_{\theta_{\min}/2}^{1} dx \frac{(1-x^2)^{m+n}}{x^{3-s-l}} \left((1-x^2)k^2+1\right) \left[Z - \frac{N_e}{y^2x^2+1}\right]^2 . \qquad (4.10)$$

As in the non-relativistic case, terms of order $\mathcal{O}(y\Lambda^{-1})$ are neglected. To justify this, we assume the maximum kinetic energy of an electron to be around $100\,\text{MeV}$ [5], which is around 200 times the electron rest mass. This corresponds to

$$k = \frac{p}{m_e c} = \sqrt{\left(\frac{E}{m_e c^2}\right)^2 - 1} \sim 200 \Rightarrow y \sim 300k \sim 10^5 \ll \Lambda . \qquad (4.11)$$

Figure 4.1 shows it works well to neglect the $\mathcal{O}(y\Lambda^{-1})$ terms up to the maximum considered momentum at $k = 100$. By extending the interval for k (figure not shown here for brevity), we find that the non-screened limit is not reached until around $k \sim 10^6$, which consequently is where the approximation $y\Lambda^{-1} \ll 1$ breaks down.
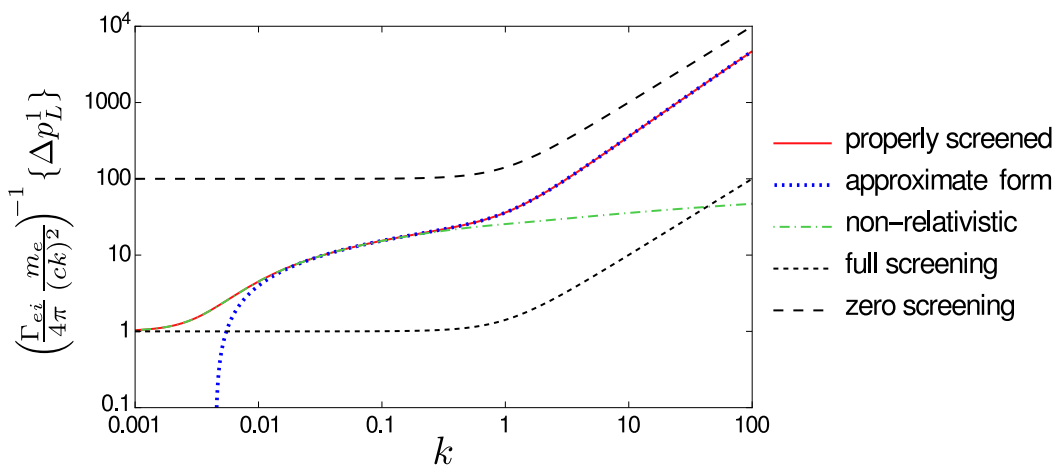
Figure 4.1: The momentum moment $\{\Delta p_L^1\}$ as a function of normalized momentum $k = p/(m_e c)$ with k^2 in eq. (4.12) multiplied out for the clarity of plotting. The following parameters were used: $X = 10$, $\ln \Lambda = 20$, $a = a_0$ and the prefactor $(\Gamma_{ei} m_e)/(4\pi c^2)$ set to unity. The relativistic expression accounting for screening is seen in solid red, with its high-momentum approximate form shown in dotted blue. The non-relativistic version is represented by dash-dotted green. The relativistic limits of full and zero screening are denoted by dashed and long dashed black lines respectively. For a large part of the interval, both the approximate and non-relativistic versions follow the full result closely. The large momentum approximation deviates at low momentum, and the non-relativistic approximation starts to deviate around $k \sim 1$. The discrepancy between assuming full screening and an accurate treatment of screening is evident.

Except for a factor of $\sqrt{1+k^2}$, the required momentum moments are similar to the non-relativistic counterparts. Eq. (4.10) leads to

$$\{\Delta p_L^1\} = -\frac{\Gamma_{ab}}{4\pi}\frac{m_e}{(ck)^2}\sqrt{1+k^2}\left[1+\frac{g_{\mathrm{rel}}(y)}{\ln\Lambda}\right],\tag{4.12}$$

$$\{\Delta p_L^1\Delta p_L^1\} = \frac{\Gamma_{ab}}{4\pi}\frac{m_e^2}{ck}\sqrt{1+k^2}\frac{l_{\mathrm{rel}}(y)}{\ln\Lambda},\tag{4.13}$$

$$\{\Delta p_L^2\Delta p_L^2\} = \{\Delta p_L^3\Delta p_L^3\} = \frac{\Gamma_{ab}}{4\pi}\frac{m_e^2}{ck}\sqrt{1+k^2}\left[1+\frac{h_{\mathrm{rel}}(y)}{\ln\Lambda}\right],\tag{4.14}$$

where we have used $\gamma = \sqrt{k^2+1}$ and

$$\begin{aligned}g_{\mathrm{rel}}(y) =&\frac{1}{2}\left(X^2-1\right)\ln\left(y^2+1\right) - \frac{(X-1)^2}{k^2+1}\frac{y^2}{2\left(y^2+1\right)}\\&-\frac{k^2}{k^2+1}\left[\left(X^2-X+\frac{1}{2}\right) - X(X-1)\frac{\ln\left(y^2+1\right)}{y^2}\right],\end{aligned}\tag{4.15}$$

$$\begin{aligned}l_{\mathrm{rel}}(y) =&2\left[\frac{X^2}{4}\frac{(k^2+2)}{(k^2+1)} - X(X-1)\frac{\ln\left(y^2+1\right)}{y^2} + \frac{(X-1)^2}{k^2+1}\frac{1}{2\left(y^2+1\right)}\right.\\&\left.+\frac{k^2}{2y^2(k^2+1)}\left(3X^2-4X+1\right)\left(1-\frac{\ln\left(y^2+1\right)}{y^2}\right)\right],\end{aligned}\tag{4.16}$$

$$h_{\mathrm{rel}}(y) = g_{\mathrm{rel}}(y) - \frac{1}{2}l_{\mathrm{rel}}(y).\tag{4.17}$$

The expressions $g_{\mathrm{rel}}(y)$, $h_{\mathrm{rel}}(y)$ and $l_{\mathrm{rel}}(y)$ are lengthy, but a high-momentum approximate form (assuming $y \gg 1$) is, as shown in Figure 4.1, in good agreement with the full expressions upwards from the thermal speed,

$$g_{\mathrm{rel}}(y) \rightarrow \left[\left(X^2-1\right)\ln(y) - \frac{k^2X^2}{2\left(k^2+1\right)} - \frac{1}{2}(X-1)^2\right],\tag{4.18}$$

$$l_{\mathrm{rel}}(y) \rightarrow \frac{X^2}{2}\left(\frac{k^2+2}{k^2+1}\right).\tag{4.19}$$

We see these asymptotic forms are similar to the non-relativistic versions (eqs. (3.28)-(3.30)).

For comparison, the fully screened expressions given up to the leading order in $\ln\Lambda$ are

$$\{\Delta p_L^1\}_{\mathrm{fs}} = -\frac{\Gamma_{ab}}{4\pi}\frac{m_e}{(ck)^2}\sqrt{1+k^2},\tag{4.20}$$

$$\{\Delta p_L^2\Delta p_L^2\}_{\mathrm{fs}} = \{\Delta p_L^3\Delta p_L^3\}_{\mathrm{fs}} = \frac{\Gamma_{ab}}{4\pi}\frac{m_e^2}{ck}\sqrt{1+k^2}.\tag{4.21}$$

The above results are summarized in Figure 4.1, where the full relativistic result for $k^2\{\Delta p_L^1\}$ in eq. (4.12) is shown and compared to the limits of full and vanishing screening, as well as to the approximate form using eq. (4.18) and the non-relativistic result in eq. (3.25). The behavior of $k\{\Delta p_L^2\Delta p_L^2\}$ is both qualitatively and quantitatively similar to $k^2\{\Delta p_L^1\}$, while $k\{\Delta p_L^1\Delta p_L^1\}$ is smaller, as in the non-relativistic

case. The chosen range for k corresponds to the relevant part of phase space: from a sub-thermal velocity up to a very energetic runaway electron (note E is the total energy, $10\,\mathrm{eV}$ and $100\,\mathrm{MeV}$ concerns the kinetic energy)

$$k = \frac{p}{m_e c} = \sqrt{\left(\frac{E}{m_e c^2}\right)^2 - 1} \Rightarrow \begin{cases} 10\,\mathrm{eV} \leftrightarrow k \sim 10^{-2}, \\ 100\,\mathrm{MeV} \leftrightarrow k \sim 10^2. \end{cases} \tag{4.22}$$

Already at small momentum, around $k = 0.01$ which would typically correspond to the thermal speed in a cold plasma, a significant difference between the full treatment of screening and the assumption of full screening can be seen. The relativistic treatment can be seen to become important when $k \sim m_e c$, i.e. where the factor of $\sqrt{1 + k^2}$ becomes large compared to unity.

As in the non-relativistic case in Section 3.2.1, the collision frequencies are most easily parametrized by the functions $g_{\mathrm{rel}}(y)$, $h_{\mathrm{rel}}(y)$ and $l_{\mathrm{rel}}(y)$. We obtain the electron-ion collision frequencies

$$\nu_D^{ei} = \frac{n_i}{c^3} \frac{\Gamma_{ei}}{4\pi} \frac{1}{k^3} \sqrt{1 + k^2} \left(1 + \frac{h_{\mathrm{rel}}(y)}{\ln \Lambda}\right), \tag{4.23}$$

$$\nu_S^{ei} = \frac{n_i}{c^3} \frac{\Gamma_{ei}}{4\pi} \frac{1}{k^3} \frac{1}{\ln \Lambda} \frac{1}{y} \frac{\partial}{\partial y} \left(\frac{1}{2} l_{\mathrm{rel}}(y) y^2 \sqrt{1 + k^2}\right), \tag{4.24}$$

$$\nu_{\parallel}^{ei} = \frac{n_i}{c^3} \frac{\Gamma_{ei}}{4\pi} \frac{\sqrt{1 + k^2}}{k^3} \frac{l_{\mathrm{rel}}(y)}{\ln \Lambda}. \tag{4.25}$$

We may compare these collision frequencies to their fully screened limits, as well as to the corresponding electron-electron collision frequencies. Regarding the fully screened collision frequencies, only $\nu_{D,\mathrm{fs}}^{ei}$ (obtained in the limit of large $\ln \Lambda$ of eq. (4.23)) is non-zero, in the infinite mass and stationary ion limit. The electron-electron collision frequencies are known from [6, 33] (note that they cannot be obtained from the above, due to the assumption of infinite mass ratio). In the high energy limit they are given by

$$\nu_D^{ee} = \frac{n_e}{c^3} \frac{\Gamma_{ee}}{4\pi} \frac{\sqrt{k^2 + 1}}{k^3}, \tag{4.26}$$

$$\nu_S^{ee} = \frac{n_e}{c^3} \frac{\Gamma_{ee}}{4\pi} \frac{k^2 + 1}{k^3}, \tag{4.27}$$

$$\nu_{\parallel}^{ee} = 0. \tag{4.28}$$

Note that the difference between Γ_{ei} and Γ_{ee} defined in eq. (2.46) is merely a factor of Z_0^2. For the singly ionized case, we have $n_e = n_i$ and therefore

$$\nu_{D,\mathrm{fs}}^{ei} = \nu_D^{ee}. \tag{4.29}$$

For this singly ionized case, the three collision frequencies in eqs. (4.23)-(4.25) are shown in Figure 4.2, along with the electron-electron frequencies in eqs. (4.26)-(4.28). There is a significant enhancement of the deflection frequency ν_D^{ei} compared to the corresponding electron-electron frequency ν_D^{ee}, and thus, by eq. (4.29), also in comparison to the fully screened deflection frequency $\nu_{D,\mathrm{fs}}^{ei}$. Since the effect is

most notable at high momentum (almost two orders of magnitude), this could affect runaway electrons in particular. At low and intermediate momentum, the slowing-down collision rate ν_S^{ei} is slightly larger than the same electron-electron frequency ν_S^{ee}, although at very high momentum ν_S^{ee} is largely dominating.
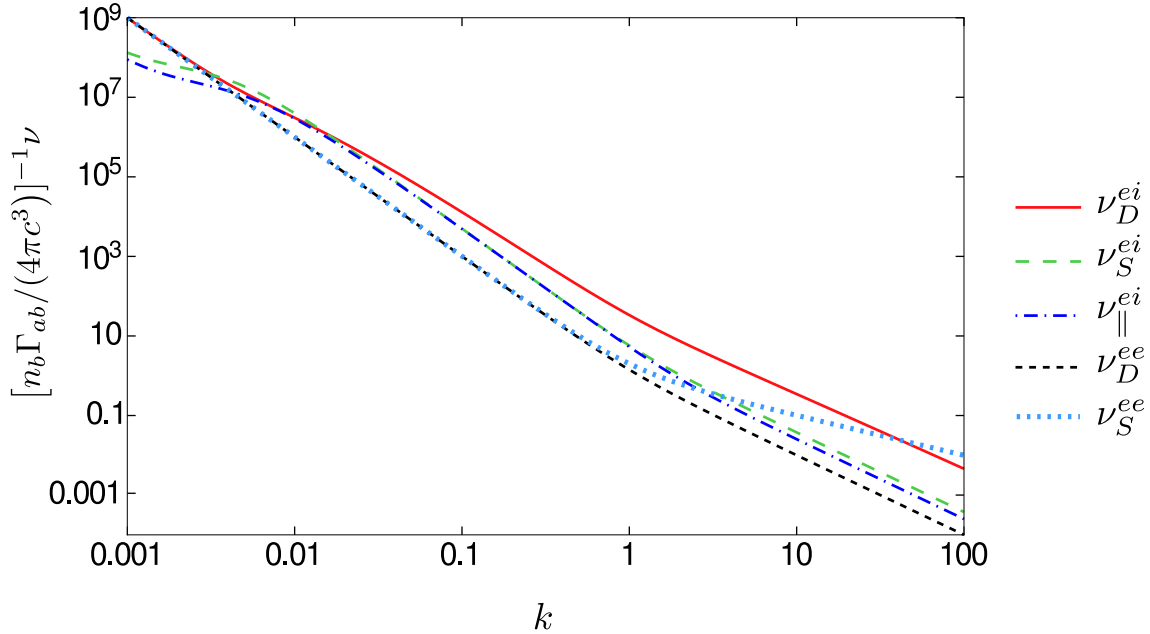
Figure 4.2: The three electron-ion collision frequencies ν_D^{ei} (solid red), ν_S^{ei} (long dashed green) and $\nu_\parallel^{ei}$ (dash-dotted blue) plotted as a function of normalized momentum $k = p/(m_e c)$ and compared to the electron electron collision frequencies ν_D^{ee} (dashed black) and ν_S^{ee} (dotted blue). Note that for single ionization, $Z_0 = 1$, the deflection frequency $\nu_D^{ee} = \nu_{D,\mathrm{fs}}^{ei}$, the fully screened deflection frequency. The chosen parameters were $X = 10$, $\ln \Lambda = 20$, $Z_0 = 1$ and $a = a_0$. The collision frequencies are normalized by setting $n_b \Gamma_{ab}/(4\pi c^3) = 1\,\mathrm{s}^{-1}$. At highly relativistic momenta, the deflection frequency ν_D^{ei} is enhanced by almost two orders of magnitude (X^2) compared to the fully screened formula. Though both ν_S^{ei} and $\nu_\parallel^{ei}$ are zero in the fully screened theory, here we see they are comparable to the electron-electron collision frequencies through most of the region, and even comparable to ν_D^{ei} in a small region.

Through most of the region in Figure 4.2, the deflection frequency ν_D^{ei} dominates over the other two electron-ion frequencies, which is expected from the asymptotic forms of eqs. (4.18) and (4.19), however the slowing-down and parallel frequencies ν_S^{ei} and $\nu_\parallel^{ei}$ are not negligible compared to the deflection frequency, except at very high momentum. This gives the impression that our corrections significantly alter the dynamics, since ν_S^{ei} and $\nu_\parallel^{ei}$ vanish identically in the limit of infinite ion mass compared to the electron mass. In contrast, recall from Section 3.2.2 the energy loss due to these slowing-down and parallel collision frequencies is zero in the heavy ion limit. This result does not apply in the relativistic case. Since the relativistic kinetic energy takes a different form compared to the non-relativistic case ($E = (\gamma - 1)mc^2 = (\sqrt{1 + k^2} - 1)mc^2 \xrightarrow[k \to 0]{} k^2 mc^2/2$), the contributions from the two frequencies ν_S^{ei} and $\nu_\parallel^{ei}$ do not cancel. Consequently, the screened Fokker–Planck

operator exhibits energy diffusion and causes energy transfer between species. Since a kinematic treatment shows that energy cannot be transferred between particles in the limit of infinite mass ratio, the parallel diffusion rates caused by these two collision frequencies are not physical.

Interestingly, previous works have only considered the correction of the deflection frequency due to incomplete screening [17, 19]. By neglecting the effect of $\{\Delta p_L^1 \Delta p_L^1\}$ (and thus also the difference between $p\{\Delta p_L^2 \Delta p_L^2\}$ and $p^2\{\Delta p_L^1\}$), corrections to the (for full screening) vanishing ν_S^{ei} and $\nu_\parallel^{ei}$ will not be found. One may question the generality of our results – could the chosen model for bound electron density have a large impact on the collision frequencies? Quite the opposite, these unphysical terms do arise also in the fully screened Fokker–Planck collision operator, but can then be neglected due to the large value of $\ln \Lambda$. In our case the same approximation does not apply: the factor $X^2/\ln \Lambda$ is typically larger than unity. On one hand, the Coulomb logarithm is connected to the dominance of small-angle collisions. On the other hand, small angle collisions are less dominant in the transition from full screening to no screening, as pointed out in Section 3.2. Whether this unphysical energy transfer between particles in individual collisions points to a fundamental problem with the Fokker–Planck operator or means that large-angle collisions are suppressed to a lesser extent in these circumstances remains unknown; further investigation of the issue is needed.

We can finally note some general characteristics of the behavior at high momentum. The general argument of Section 3.3.4 applies also to the relativistic case, and using the high momentum forms of eqs. (4.18) and (4.19) we obtain

$$\nu_D^{ei} = \nu_{D,\text{fs}}^{ei} \left[(X^2 - 1)\ln(y) + \text{const} \right]. \tag{4.30}$$

The same behavior, both regarding the scaling with ionization degree and momentum, was determined in Refs. [17, 19], where the semi-classical Tomas-Fermi model of the bound electron density (as discussed in the Introduction) of the ion was used. By fixing our free parameter a, which is related to the size of the atom and included in the momentum parameter $y \propto (a/a_0)k$, see eq. (3.6), the constant difference could be absorbed. The two different approaches, using either the Yukawa model or the Thomas–Fermi theory to describe the bound electron density, thus give the same results for screening in the Fokker–Planck treatment. This is again a sign that the collision operator is fairly insensitive to the details of the form factor derived from the electron density of the ion.

5
Conclusions

The phenomenon of runaway electrons is an interesting area of plasma physics. The study of runaways has practical importance, as, for example, they pose a great threat to fusion reactors. Realistic scenarios often require a description of the interaction between runaway electrons and partially ionized heavy atoms. The strength of the Coulomb interaction depends on the electron momentum, as a high momentum electron can penetrate the electron cloud around the nucleus and thus experience a higher charge compared to the fully screened case. Since the cross section scales as the square of the charge, this may have a strong effect on the runaway electron dynamics where collisional effects are important.

This thesis focused on describing collisions with ions in a way that properly takes screening into account. An accessible, independent derivation of the collision operator was provided. Unlike previous works, we included a thorough analysis of the validity of the Fokker–Planck operator and electron density sensitivity. Starting from the quantum mechanical cross sections, the non-relativistic Fokker–Planck operator was derived assuming a Yukawa-type model for the distribution of the bound electron density around the nucleus. Furthermore, the relativistic counterpart was derived in the limit of infinite ion to electron mass ratio. The robustness of the results was analyzed by two different approaches. The validity of the Fokker–Planck collision operator was investigated by comparing the Fokker–Planck terms to higher order terms in the expansion of the Boltzmann operator. When small deflection-angle collisions dominate, the higher order terms should be small. We found an intermediate region between low and high momentum where higher order corrections to the Fokker–Planck theory are more important. This indicates that there are situations where a Boltzmann treatment would be beneficial, in particular for a low degree of ionization.

Moreover, the sensitivity of the results to the bound electron density model was investigated by considering a second, qualitatively different electron density model and looking for the general model-independent, high-momentum behavior. The Fokker–Planck operator was shown to be insensitive to the exact form of the electron density. Particularly at high momentum, the collision frequencies show a logarithmic momentum dependence, and the model of the bound electron density merely provides a length scale. Since the main application of this project involves high momentum corrections, this is an important result which indicates that our conclusions are reliable. In order to get this scale parameter correctly, it would however still be valuable to investigate other, more sophisticated bound electron density mod-

els. One step towards a more accurate description is obtained by the semi-classical Thomas–Fermi model, however it is desirable to consider the quantum mechanical density functional theory to achieve a significantly more accurate description than our present model [34, 35].

As expected, we find a considerable enhancement of the electron-ion collision rates when accounting for screening effects. Of greatest important in fusion experiments is likely to be the enhancement of the pitch angle scattering, in which the energy of the electron is conserved but the direction of motion changes. This will cause increased energy loss of runaway electrons in the magnetized plasmas of interest for controlled fusion, due to the synchrotron radiation process. Numerical solution of the kinetic equation will however be necessary in order to obtain quantitative results regarding the dynamics of runaways. In particular, it would be of great interest to investigate the effects on the growth rate of runaway electron density and the momentum-space structure of the electron distribution function.

An apparently peculiar result regards the scaling of our screened nuclei corrections with mass. In the limit of light electrons interacting with heavy ions, the energy transfer between the two species should be negligible. In contrast, we find that while the non-relativistic operator does not transfer energy between the species, it still has diffusive properties implying that energy is transferred between particles in individual collisions. The situation is most marked for the relativistic operator, where there is a net transfer of energy in the heavy ion limit from the electron species to the ion species. Since our results inherently come with a prefactor of the inverse Coulomb logarithm $\ln \Lambda$, the terms producing this effect are usually neglected (as discussed in Section 2.2.3). In the situations of interest in this thesis, that is heavy ions of low ionization degree, our corrections are however rather large and cannot be neglected in the usual fashion.

It is intriguing that the higher order term in the inverse Coulomb logarithm produces this unphysical result. While the leading order $1/\ln \Lambda$ terms are closely connected to the domination of small-angle scattering, the higher order term is related to large angle scattering, where the Fokker–Planck operator is not valid. The unphysical energy diffusion in the heavy ion limit is therefore an artefact of the Fokker–Planck theory, due to the truncation of the Taylor-expanded Boltzmann operator. To our knowledge, this has not been investigated previously.

Combined with the analysis of the higher order terms of the Taylor-expanded Boltzmann operator, we therefore see a theoretical need to investigate scattering through any angle and not just consider small-angle scattering as in the Fokker–Planck theory. Additionally, it is well known that large-angle collisions play an important role in the growth of the runaway population. Large-angle collisions must be treated with the Boltzmann operator instead of within the Fokker–Planck framework. Though usually considerably more complicated to deal with, it will be of great interest to consider the Boltzmann operator and determine how it alters the picture.

We would therefore suggest further development in several directions. As a continuation of the present work, an investigation of more accurate electron densities could be undertaken. Since the effect on the electron distribution function due to collisions

between electrons and partially ionized ions has not been investigated thoroughly in the literature, it would also be valuable to implement the present results in an existing kinetic equation solver, such as CODE [6]. To complete the picture of scattering by a partially ionized ion, the elastic collisions considered herein should be complemented by the description of inelastic scattering, as mentioned in Section 2.3.1, since interaction with the bound electrons of the ion may cause a change in the ion energy state. Finally, and more fundamentally, a Boltzmann operator treatment of the problem would be valuable.

Bibliography

[1] F. Chen, *Introduction to Plasma Physics and Controlled Fusion.* Plenum Press, 1984.

[2] P. Helander and D. Sigmar, *Collisional Transport in Magnetized Plasmas.* Cambridge Monographs on Plasma Physics. Cambridge University Press, 2005.

[3] P. Helander, L.-G. Eriksson, and F. Andersson, *Runaway acceleration during magnetic reconnection in tokamaks, Plasma Physics and Controlled Fusion* **44** (2002) B247.

[4] J. R. Dwyer, *Relativistic breakdown in planetary atmospheres, Physics of Plasmas* **14** (2007) 042901.

[5] E. M. Hollmann, P. B. Parks, N. Commaux, N. W. Eidietis, R. A. Moyer, D. Shiraki, M. E. Austin, C. J. Lasnier, C. Paz-Soldan, and D. L. Rudakov, *Measurement of runaway electron energy distribution function during high-Z gas injection into runaway electron plateaus in DIII-D, Physics of Plasmas* **22** (2015) 056108.

[6] M. Landreman, A. Stahl, and T. Fülöp, *Numerical calculation of the runaway electron distribution function and associated synchrotron emission, Computer Physics Communications* **185** (2014) 847.

[7] C. T. R. Wilson, *The acceleration of β-particles in strong electric fields such as those of thunderclouds, Mathematical Proceedings of the Cambridge Philosophical Society* **22** (1925) 534.

[8] H. Dreicer, *Electron and ion runaway in a fully ionized gas. I, Phys. Rev.* **115** (1959) 238.

[9] H. Dreicer, *Electron and ion runaway in a fully ionized gas. II, Phys. Rev.* **117** (1960) 329.

[10] M. Kruskal and I. B. Bernstein, *Princeton Plasma Physics Lab, Report no. MATT-Q-20* (1962) 172.

[11] J. Connor and R. Hastie, *Relativistic limitations on runaway electrons, Nuclear fusion* **15** (1975) 415.

[12] R. M. Kulsrud, Y.-C. Sun, N. K. Winsor, and H. A. Fallon, *Runaway electrons in a plasma*, *Phys. Rev. Lett.* **31** (1973) 690.

[13] M. Rosenbluth and S. Putvinski, *Theory for avalanche of runaway electrons in tokamaks*, *Nuclear Fusion* **37** (1997) 1355.

[14] ITER organization. `http://www.iter.org`. Accessed: 2016-03-09.

[15] E. Hollmann, M. Austin, J. Boedo, N. Brooks, N. Commaux, N. Eidietis, D. Humphreys, V. Izzo, A. James, T. Jernigan, A. Loarte, J. Martin-Solis, R. Moyer, J. Muñoz-Burgos, P. Parks, D. Rudakov, E. Strait, C. Tsui, M. V. Zeeland, J. Wesley, and J. Yu, *Control and dissipation of runaway electron beams created during rapid shutdown experiments in DIII-D*, *Nuclear Fusion* **53** (2013) 083004.

[16] J. R. Martín-Solís, A. Loarte, and M. Lehnen, *Runaway electron dynamics in tokamak plasmas with high impurity content*, *Physics of Plasmas* **22** (2015) 092512.

[17] K. Aleynikova, P. Aleynikov, S. Konovalov, A. Teplukhina, and V. Zhogolev, *Interaction of runaway electrons with high-Z impurities*, in *40th European Physical Society Conference on Plasma Physics, Espoo, Finland*, O5.103, 2013.

[18] V. Zhogolev and S. Konovalov, *Characteristics of interaction of energetic electrons with heavy impurity ions in a tokamak plasma*, *VANT or Problems of Atomic Sci. and Tech. series Thermonuclear Fusion* **37** (2014) 71. (in Russian).

[19] Y. L. Igitkhanov, *The effect of non-Coulomb scattering of relativistic electrons on the generation of runaways in multicomponent plasma*, *Contributions to Plasma Physics* **52** (2012) 460.

[20] V. D. Kirillov, B. A. Trubnikov, and S. A. Trushin, *Role of impurities in anomalous plasma resistance*, *Fizika Plazmy* **1** (1975) 218.

[21] D. Mosher, *Interactions of relativistic electron beams with high atomic-number plasmas*, *Physics of Fluids* **18** (1975) 846.

[22] L. D. Landau and E. M. Lifshitz, *Quantum mechanics: non-relativistic theory*, vol. 3. Elsevier, 2013.

[23] H. Akama, *Relativistic Boltzmann equation for plasmas*, *Journal of the Physical Society of Japan* **28** (1970) 478.

[24] D. Montgomery and D. Tidman, *Plasma Kinetic Theory*. McGraw-Hill advanced physics monograph series. McGraw-Hill, 1964.

[25] F. Hinton, *Collisional transport in plasma*, in *Basic plasma physics*, vol. 1. Amsterdam: North-Holland Publishing Company, 1983.

[26] L. D. Landau, *24 - The transport equation in the case of Coulomb interactions*, in *Collected Papers of L.D. Landau* (D. T. Haar, ed.), p. 163. Pergamon, 1965.

[27] M. N. Rosenbluth, W. M. MacDonald, and D. L. Judd, *Fokker-planck equation for an inverse-square force*, Phys. Rev. **107** (1957) 1.

[28] J. J. Sakurai, *San Fu Tuan. Modern quantum mechanics*. Reading, Mass.: Addison-Wesley Pub. Co, 1994.

[29] W. Heitler, *The quantum theory of radiation*, vol. 86. Courier Corporation, 1954.

[30] S. Weinberg, *Gravitation and Cosmology*. John Wiley and Sons, New York, 1972.

[31] S. M. Carroll, *Lecture notes on general relativity*, 1997.
arXiv:gr-qc/9712019.

[32] J. E. Sansonetti and W. C. Martin, *Handbook of basic atomic spectroscopic data*, *Journal of Physical and Chemical Reference Data* **34** (2005) 1559.

[33] G. Papp, M. Drevlak, T. Fülöp, and P. Helander, *Runaway electron drift orbits in magnetostatic perturbed fields*, *Nuclear Fusion* **51** (2011) 043004.

[34] W. Kohn and L. J. Sham, *Self-consistent equations including exchange and correlation effects*, Phys. Rev. **140** (1965) A1133.

[35] P. Hohenberg and W. Kohn, *Inhomogeneous electron gas*, Phys. Rev. **136** (1964) B864.

Bibliography